ENSO and Eddy Energetics along the Tropical Storm Track

Part I : Eddy Energetics

1. Introduction for Part I

El Niño-Southern Oscillation (ENSO), a highly coupled air-sea system, may affect the interannual variability of the tropical storms (TSs) over the western North Pacific (WNP) by altering the thermodynamic and dynamic states of the large-scale environments in which TSs are formed and propagate. (e.g., see the reviews in Landsea 2000 and Chan 2005). One of the important large-scale environments that affect the position of tropical storm genesis is the monsoon trough (Gray 1979; McBride 1995). It can increase low-level vorticity and provide a favorable environment for the growth and development of tropical storms. A statistical analysis of the classifiable genesis proposed by Ritchie (1995) indicated that more than 75% of tropical cyclone genesis occurred in the monsoon trough.

Chen et al. (1998), Chia and Ropelewski (2002), Wang and Chan (2002) and Chen et al. (2006) all noticed that during El Niño (La Niña) years, the warm sea surface temperature (SST) and monsoon trough extends (retreats) southeastward (westward). These conditions provide a favorable environment for the formation and development of tropical cyclone in the southeast (northwest) region of the WNP during El Niño (La Niña) years (Chia and Ropelewski 2002; Wang and Chan 2002). The shift in the location of TS formation associated with ENSO events may indirectly influence the intensity (Chan and Liu 2004; Camargo and Sobel 2005) and life span of the tropical storm (Wang and Chan 2002). Tropical storms tend to have longer life spans (Wang and Chan 2002), and are stronger during El Niño years (Chan and Liu 2004; Camargo and Sobel 2005).

While shifts in genesis location, longer life span and greater intensity of TS

during El Niño years appear to be related, the relationship and interaction between the mean flow environment and tropical storm characteristics are not fully understood (Camargo and Sobel 2005). Camargo and Sobel (2005) suggested that the variation in TS intensity might be due, in part, to other effects of ENSO on the mean regional climate of the WNP. The numerical experiments performed by Li (2006) indicate that in the absence of perturbation convective heating and convection-frictional convergence feedback, summer mean flow alone is unable to lead to the synoptic-scale perturbation growth.

To understand the interaction between the mean flow environment and transient eddies, this study investigated the energy processes between the tropical mean flow and the tropical eddies including tropical storms during different ENSO phases. Following the pioneer work of Lorenz (1955), who developed the concept of available potential energy (APE), the traditional energy form is decomposed into zonal mean flow and deviations from it, as eddies. It has been widely applied to investigate the general circulation of atmosphere for closed systems (e.g. Lorenz 1967; Oort 1964; Kung 1966; Hu et al. 2004), extratropical cyclones (Kung 1977; Robertson and Smith 1983) and African easterly wave (Norquist et al. 1977; Hsieh and Cook 2007) for open systems. On the other hand, fewer studies have partitioned the kinetic and available potential energy in the time domain to understand the energy conversions between the time-mean flow and transient mode for open domains. Based on the three-dimensional eddy kinetic energy (KE) analysis and the simplified two-dimensional eddy APE budget equation partitioned in the time domain within a limited region, Lau and Lau (1992) noted that the local barotropic energy conversion between the mean flow and transient eddies at low-levels could intensify the 3-10 day

transient eddies associated with tropical cyclogenesis. Using the perturbation KE and APE tendency equations in a manner similar to that of Lau and Lau (1992), Maloney and Dickinson (2003) found that both the barotropic and baroclinic energy conversions increase during the Madden and Julian oscillation (MJO) westerly phase, which favor the eddy growth and tropical cyclone formation.

In the tropics, both Walker circulation and Hadley cell change significantly during ENSO warm and cold years. The modulation of Walker circulation associated with ENSO may not be represented by the zonal mean process which precludes longitudinal variation. It may be appropriate to divide the energy forms into time mean and eddy energy forms for investigating the interaction between background mean flow and the development of transient disturbances including tropical storms. Thus, the three-dimensional eddy KE and APE energy budget equations partitioned in the time domain were applied in this study to investigate the energy processes over the WNP during ENSO warm and cold phases. The data and analytical method are described in section 2. The three-dimensional eddy kinetic energy (EKE) and eddy available potential energy (EAPE) budget equations applied in this study are presented in section 3. The results of the interannual variability of large-scale circulations and tropical storms over the WNP are presented in section 4. The energy processes for generation and maintenance of the APE and KE of eddies are examined in section 5. A summary of eddy energetics (Part I) is presented in section 6.

2. Data and analysis methods

2.1 Data

The National Centers for Environmental Prediction (NCEP) - Department of Energy (DOE) reanalyses (Kanamitsu et al. 2002) from 1979 to 1998 were used in this study to examine large-scale circulations and eddy energetics over the WNP. The horizontal resolutions of these thermodynamic and dynamic variables are 2.5° longitudes by 2.5° latitudes. These data are utilized at 17 pressure levels, ranging from 1000 hPa to 10 hPa. The monthly Sea Surface Temperature (SST) with 2°×2° resolution obtained from the NCEP-NCAR (Reynolds and Smith 1994) was also adopted in this study for classification of ENSO events.

The 6-hourly best track data of tropical cyclones published by the Joint Typhoon Warning Center (JTWC 2008) were obtained for examination of the interannual variability of TS activity over the WNP. Only those tropical cyclones with a maximum wind speed of at least 17m/s (intensity of tropical storms) were considered in the calculation of TS frequency and other TS activity indices.

2.2 Classification of warm and cold ENSO years

Wang and Chan (2002) found that the relationship between TS activity and the Pacific SST depends on the location of SST anomalies. Among different Niño indices, the Niño3.4 sea surface temperature anomaly (SSTA) is better correlated with TS activity over the WNP, because the occurrence of organized convection depends on the total SST and SST gradient, rather than on the SST anomaly itself. In addition,

they found that the correlation between the interannual variability of tropical storms over the WNP and Niño3.4 SSTA has a strong seasonal dependence. During TS peak season (July-September), TS activity is closely related to Niño3.4 SSTA during July-September, although the ENSO forcing is strongest during the winter (Wang and Chan 2002; Chan 2005). Therefore, the ENSO classification in this study were stratified by the July-September SSTA in the Niño3.4 region into warm years (SSTA $\geqq$ 0.8 standard deviation), cold years (SSTA $\leqq$ -0.8 standard deviation) and normal years (-0.8 standard deviation < SSTA < 0.8 standard deviation). Based on these criteria, four major warm (1982, 1987, 1991, 1997) and cold (1981, 1985, 1988, 1998) years were identified during the period from 1979 to 1998.

3. Diagnostic energetic equations

3.1 Eddy kinetic and available potential energy equations

The diagnostic tool adopted in this study is a primitive equation (PE) form of the three-dimensional eddy kinetic energy and available potential energy equations for an open system. To investigate meridional, as well as longitudinal, variation associated with ENSO, we used the concept of available potential energy developed by Lorenz (1955), but partitioned the kinetic and available potential energy into the time domain. The eddy kinetic energy (EKE, K') and the eddy available potential energy (EAPE, A') can be expressed as (1) and (2), respectively.

$$K' = \frac{1}{2}(\overline{u'^2} + \overline{v'^2}) \tag{1}$$

$$A' = \frac{c_p}{2}\int_0^{\infty} \gamma \frac{\overline{T'^2}}{[\overline{T}]}\, dp \tag{2}$$

In the above expression, the symbol, "$\overline{\ }$", represents the time mean from July to September, while " $'$ " is the deviation from the July-September time mean. The variables u and v are the zonal and meridional wind fields, respectively. "[ ]" represents the global average and "*" represents the deviation from the global average. T is the temperature and c_p is the specific heat at constant pressure. γ is defined as $\Gamma_d/(\Gamma_d - [\Gamma])$, and $\Gamma_d = g/c_p$ and $\Gamma = -\partial T/\partial z$ are dry-diabatic and environmental lapse rates, respectively.

To derive the EKE and EAPE energy equations, we first multiplied the eddy

momentum equations by u', v' and thermodynamic equation by $(\frac{P}{P_0})^{2\kappa}\frac{c_p}{[T]}\gamma\theta'$, respectively. Then, we added the two momentum equations associated with the eddy kinetic energy equation and applied both the continuity and hydrostatic equations to the resulting equations. Finally, the budget equations of EKE and EAPE for an open system can be written as equations (3) and (4), respectively, which are similar to those from Oort (1964), but include boundary flux terms.

$$\frac{\partial K'}{\partial t} = \underbrace{-\overline{(V'\cdot(V_3'\cdot\nabla_3)\overline{V})}}_{C_K} \underbrace{-\frac{R}{P}\overline{T'\omega'}}_{C_E} \underbrace{-\overline{V_3}\cdot\nabla_3\overline{K'} - \overline{V_3'\cdot\nabla_3 K'}}_{B_{K'}} \underbrace{-\overline{\nabla_3\cdot(V_3'\phi')}}_{B_{\phi'}} + D \tag{3}$$

$$\frac{\partial A'}{\partial t} = \underbrace{-\frac{c_p}{[\overline{T}]}\gamma\left[\overline{T'(V'\cdot\nabla)\overline{T}} + (\frac{P}{P_0})^{\kappa}\overline{T'\omega'}\frac{\partial\overline{\theta}^*}{\partial p}\right]}_{C_A} \underbrace{+\frac{R}{P}\overline{T'\omega'}}_{-C_E} \underbrace{-\overline{V_3}\cdot\nabla_3\overline{A'} - \overline{V_3'\cdot\nabla_3 A'}}_{B_{A'}} \underbrace{+\frac{\gamma}{[\overline{T}]}\overline{T'Q'}}_{G_{A'}} \tag{4}$$

where t is time, V is the horizontal velocity vector, and $\bigtriangledown$ is the horizontal gradient operator (the suffix 3 presents the three-dimensional components), $\omega = dP/dt$ vertical velocity, P is pressure, ϕ is geopotential, θ is potential temperature, $\kappa \equiv R/c_p$, and Q is diabatic heating rate.

The physical mechanisms of the eddy energy generation and conversion processes can be explained as follows. The term, C_K, represents the eddy barotropic energy conversion from mean kinetic energy (MKE) to EKE. C_E is referred to as eddy baroclinic energy conversion from EAPE to EKE. This term is identical to the

generation of EKE in a closed system. For an open domain in the present study, C_E can be regarded as the sum of the generation of EKE and $B_{\phi'}$, where term $B_{\phi'}$ represents the boundary flux by eddy geopotential. Terms $B_{K'}$ and $B_{A'}$ indicate the boundary flux terms of eddy kinetic energy and eddy available potential energy by the mean flow and eddies, respectively. D presents EKE dissipation by frictional and subgrid-scale effects. C_A is the energy conversion from MAPE to EAPE. Only the horizontal component of this term was used in the study by Lau and Lau (1992). In contrast, the present study compared the contributions from the horizontal and vertical components of this term. $G_{A'}$ represents the generation of EAPE. Diabatic heating, Q, of this term was estimated from the thermodynamic energy equation.

The matter of greatest interest in this study is the source of eddy kinetic energy and eddy available potential energy associated with transient eddy formation and development. Thus, we focused on the eddy kinetic and available potential energy generation and conversion processes, including C_K, C_E, C_A and $G_{A'}$.

3.2 Diabatic heating calculation

The diabatic heating Q in the EAPE budget equation (4) is estimated from the thermodynamic energy equation:

$$Q = c_p \frac{\partial T}{\partial t} + c_p (V \cdot \nabla T - \omega\sigma)$$

where $\sigma = \left(\frac{RT}{c_p P}\right) - \left(\frac{\partial T}{\partial P}\right)$ is the static stability.

Fig. 3.1 displays the vertical cross section of diabatic heating and vertical velocity over the tropical Pacific region during warm ENSO events. Significant diabatic heating and ascending motions both occur over 130°-170°E in the tropical western Pacific. The maximum values of diabatic heating and vertical motions appear in the upper-troposphere at 400 hPa (Fig. 3.1). This suggests the condensation heating associated with large-scale upward motion might be an important heat source of tropical troposphere over the WNP (Yanai et al. 1973; Lau and Lau 1992).

4. ENSO, large-scale circulation and TS activity in the WNP

The characteristics of and variation in large-scale circulation and TS activity during warm and cold ENSO years are investigated in this section. The TS activity examined in this study includes TS frequency, TS formation frequency, TS number, accumulated cyclone energy (ACE), TS life span and TS intensity. TS frequency is determined by the number of tropical storms passing over a 2.5°×2.5° grid box. The TS formation frequency is the number of TS geneses in each grid box of 2.5° latitude by 2.5° longitude. Genesis is defined as the first point for all named TS cases in the JTWC record. The definition of the ACE index (Bell et al. 2000) is the sum of the squares of the maximum sustained wind speed for all periods during which the TSs in the WNP basin (here defined as the region between 120°E-170°W and 0°-40°N). TS life span was counted by the total length of time from the first point to the last point for a named TS case in the JTWC record. The maximum surface wind speed of each TS during its entire life span was used to represent TS intensity.

Figure 4.1 depicts the frequency of tropical storms, SST and 850 hPa wind fields for warm and cold composites, respectively. Two prominent TS tracks, which were defined as the axes of the maximum and secondary maximum TS frequencies, are superimposed on Figures 4.1a-c. The primary TS tracks coincided with the monsoon trough during both warm and cold years (Figs. 4.1a and b). This result indicates that the monsoon trough, which is a low pressure region characterized by positive relative vorticity (not shown), is a vital factor for TS formation and development (Holland 1995).

The large-scale circulations, including the monsoon trough over the WNP,

undergo significant interannual variabilities associated with ENSO variation. During warm years, the monsoon trough and warmest SST region extend southeastward (Figs. 4.1a and d), while the monsoon trough and warm SST region retreat westward during the cold years (Figs. 4.1b and e), similar to the finding of Chen et al. (1998). A strong low-level westerly appears and stretches from the Bay of Bengal to the central Pacific along 5°-15°N during warm years (Fig. 4.1d). Thus, the westerly and easterly converge between 5°-10°N in the tropical central Pacific. In contrast, during cold ENSO years, the westerly retreats westward of 120°E, while the equatorial easterly strengthens and prevails over the WNP (Fig. 4.1e). Hence, the easterly and westerly convergence region between 5°-10°N migrates eastward during warm years, but westward during cold years. Accompanied by the eastward extension (westward retreat) of the monsoon trough and convergence region, the frequency of TS over the region from 150ºE to the date line dramatically increases (decreases) during the warm (cold) ENSO years (Figs. 4.1a and 1b), as discussed by Chen et al. (1998).

The differences in frequency of tropical storms, SST and circulation between the warm and cold years are shown in Figures 4.1c and 4.1f. An anomalous cyclonic (anticyclonic) circulation occurs to the northwest of warm (cold) SST anomalies over the central Pacific (western Pacific) (Figs. 4.1c and 4.1f). These atmospheric responses associated with the SST anomalies are similar to Gill's (1980) solution with a Rossby wave pattern. However, the strong anomalous westerly jet stream that appears along 0°-15°N may also induce cyclonic shear to the north of the jet. The cause of this anomalous westerly jet remains unclear. It may be related, in part, to the anomalous cyclonic circulation and the anomalous Walker circulation (Fig. 4.2), which is confined to the equator with ascending motion over the eastern Pacific and

descending motion over the western Pacific.

The low-level cyclonic vorticity (Fig. 4.3a) induced by the anomalous westerly jet and cyclonic circulation might be beneficial for the moisture convergence and convection north of the jet. Thus, the enhanced large-scale diabatic heating and ascending motion occur north of the jet during warm years (Fig. 4.3b). These large-scale diabatic heating and ascending motions might provide favorable conditions for the southward and eastward extension of the TS formation region from the tropical western Pacific to the central Pacific during warm years (Fig. 4.3a). On the other hand, the anomalous anticyclonic vorticity, diabatic cooling and descending motion that appear north of 20°N may restrict the formation of tropical storms in this region (Figs. 4.3a and b).

Once the TSs form in the southeastern part of WNP during warm years, they tend to be long-lived and have greater intensity over the ocean (Table 1), which is in agreement with the results of Wang and Chan (2002). The ACE, which represents the combined effect of the number, life span and the strength of TS, was also significantly greater during warm years than during cold years, similar to the findings of Camargo and Sobel (2005). However, TS numbers over the entire WNP during warm years were only slightly greater than during cold years (Table 1). This feature has been noticed by Wang and Chan (2002) who found that the interannual variation in TS formation number is insignificant even between strong warm and cold ENSO years. The mechanisms responsible for tropical storm genesis and development might be different. The relationship between the large-scale environment and interannual variability of TS activities over the WNP with regard to eddy energetics will be explored in the next section.

5. Eddy energetic results

5.1 Diagnosis of eddy kinetic energy

Differences in the vertically integrated kinetic energy for total, mean flow and eddy during the period from July to September between warm and cold composites are shown in Figure 5.1. Total kinetic energy increases significantly over almost the entire western North Pacific during warm years (Fig. 5.1a). Comparing the mean kinetic energy (MKE) in Fig. 5.1b and eddy kinetic energy (EKE) in Fig. 5.1c with the total kinetic energy, it is obvious that the increase in total kinetic energy is primarily associated with the increase in EKE. The increment in MKE is much less than that of EKE (Fig. 5.1c). In addition, MKE decreases in the region south of 10°N. The decrease in MKE may be partially due to the decrease in wind speed that results from the out-of-phase relationship between the anomalous westerly jet and prevailing easterly, as discussed in the previous section (Fig. 4.1f). To further explore the processes responsible for the enhanced EKE during warm ENSO years, which might contribute to transient eddies including TSs activity, the source of the EKE was examined.

Figure 5.2 depicts the vertically integrated eddy barotropic and baroclinic conversions superimposed with the TS primary track. During warm years, both the eddy barotropic and baroclinic energy conversion are positive in the region extended from the Philippine Sea (130°-150°E) to the date line (Figs. 5.2a and 5.2d), consistent with the eastward extension of the low-level westerly and convergence (Fig. 4.1d). These results are similar to those reported by Lau and Lau (1992) who demonstrated that the major energy sources for summertime synoptic-scale disturbances over the

WNP are the barotropic and baroclinic energy conversions. However, during cold years, the positive barotropic energy conversion is confined to regions westward of 140°E, in accordance with the westward retreat of the westerly jet (Fig. 4.1e). Negative values of barotropic conversion appear in the regions east of 150°E (Fig. 5.2b), which may be unfavorable for the formation of TS. Indeed, TS formation is restricted to regions west of 150°E during cold ENSO years.

As tropical storms propagated northward into subtropical regions over the western Pacific, the barotropic energy conversion became negative for both warm and cold years (Figs. 5.2a and b). This might weaken the tropical storms. Eddy baroclinic energy conversion plays an important role in the maintenance of eddy growth in the subtropical and mid-latitude regions (Figs. 5.2d and e), as reported by Kung (1977). This implies that the eddy baroclinic energy effect may strongly impact subsequent TS development. Emanuel et al. (2004) suggested that baroclinic effects may be important for the late development of hurricane intensity.

Figs. 5.2c and 5.2f show the differences in eddy barotropic and baroclinic energy conversion between warm and cold years, respectively. Apparently, both eddy barotropic and baroclinic energy conversions contribute to the growth of EKE in the region extending from the Philippine Sea (130°-150°E) to the date line during warm ENSO years. This might lead to the southeastward extension of the TS formation region, as well as the intensification of the TS from the Philippine Sea to the date line during warm years. However, the eddy barotropic energy conversion is more negative over the subtropical regions of the western Pacific during warm years than during cold years. This indicates that the large-scale environments are unfavorable for the development of eddy including TS during warm years over the subtropical WNP.

Again, eddy baroclinic energy conversion plays an important role in the maintenance and subsequent development of eddies as they propagate northward to the subtropical and mid-latitude regions.

The difference of zonal (10º-15ºN averaged) vertical cross sections of barotropic and baroclinic energy conversions over the TS formation and early-development regions for warm minus cold composites are shown in Figure 5.3. The significant increment of eddy barotropic conversion occurs at low levels, with the maximum center at 850 hPa to 950 hPa during warm years (Fig. 5.3 a). The strengthened barotropic conversion at low-level is coincided with the enhanced low-level westerly jet along 5°-15°N. The enhancement and eastward extension of the positive barotropic energy conversion associated with the low-level westerly jet during warm years play a crucial role for the growth of eddies at low-level in the TS formation and early-development regions (Fig. 5.3c). Contrary to the barotropic energy conversion, the eddy baroclinic energy conversion increases significantly at the upper levels, in agreement with Lau and Lau (1992), with a maximum anomaly at 200-300 hPa during warm events (Fig. 5.3f). The direct effect of surface heat flux associated with ENSO forcing on the eddy baroclinic energy conversion in lower troposphere is less evidence. This might be resulted from the small amplitude of vertical motion associated with eddy disturbances at low-levels.

To examine the relative importance of the eddy momentum transport associated with eddy barotropic energy conversion, each term of the barotropic energy conversion was investigated. Figure 5.4 displays the spatial distributions of vertically integrated barotropic energy conversion for each term. Because the magnitudes of

$-\overline{u'v'}\frac{\partial \bar{v}}{\partial x}$ and $-\overline{v'\omega'}\frac{\partial \bar{v}}{\partial p}$ are much smaller than the other terms (not shown), these two terms are not depicted in Figure 5.4. The enhanced barotropic energy conversion over the TS formation and early development regions during warm years is mainly contributed by the terms, $-\overline{u'^2}\frac{\partial \bar{u}}{\partial x}$ and $-\overline{u'v'}\frac{\partial \bar{u}}{\partial y}$ (Fig. 5.4a and 5.4b). The former is related to the strong zonal wind convergence ($\frac{\partial \bar{u}}{\partial x} < 0$) induced by the enhancement and eastward extension of the low-level westerly jet and monsoon trough at low levels associated with the warm ENSO years (Fig. 4.1). The importance of this term supports disturbance growth via wave accumulation mechanism (Sobel and Bretherton 1999; Kuo et al. 2001; Tam and Li 2006). Meanwhile, the latter is induced by the increment in cyclonic shear anomalies ($\frac{\partial \bar{u}}{\partial y} < 0$) associated with the strengthened low-level westerly and monsoon trough at low levels. This result indicates that the enhancement and eastward extension of the low-level westerly and monsoon trough induce a favorable environment for eddy barotropic energy conversion and wave accumulation during warm ENSO years.

The term $-\overline{u'\omega'}\frac{\partial \bar{u}}{\partial p}$ associated with the eddy vertical momentum transport also increases in the westerly jet stream region between 5°-10°N (Fig. 5.4d) at low levels during warm years. This effect not only generates eddy kinetic energy, but also reduces vertical wind shear of the mean circulation, which, in turn, may provide an environment with low vertical wind shear during the warm ENSO years.

5.2 Diagnosis of eddy available potential energy

Based on the analysis of EKE budgets in the previous subsection, eddy baroclinic energy conversion is the principal energy source responsible for the growth of EKE during warm years. Once the eddy available potential energy (EAPE) converts to EKE, it has to be replenished by other mechanisms. In this subsection, we will inspect the two major energy processes that supply of EAPE. One is energy conversion from MAPE to EAPE via eddy horizontal and vertical heat transport associated with the mean flow temperature gradients (Figs. 5.5a-c). The other is the generation of EAPE through either the heating over warm areas or cooling over cold regions (Figs. 5.5d-f). Apparently, the primary source of the EAPE is the generation of EAPE, which is consistent with many previous studies of tropical disturbances (e.g. Norquist et al. 1977; Lau and Lau 1992; Maloney and Dickinson 2003; Hsien and Cook 2007). However, energy conversion from MAPE to EAPE is significant over the WNP during both warm and cold years, although the horizontal temperature gradient in the tropics is small. In addition, both the MAPE to EAPE energy conversion and generation of EAPE increase along the TS track during warm years (Figs. 5.5c and 5.5f). These results suggest that the loss of EAPE to EKE through the eddy baroclinic energy conversion is furnished by both the generation of EAPE and the MAPE to EAPE energy conversion.

The question arises how the energy conversion from MAPE to EAPE is positive in the tropical region where the horizontal temperature gradient is small. Comparison of the relative contributions of the horizontal and vertical components of this energy process (Figs. 5.6a and b) reveals that the enhancement of energy conversion from MAPE to EAPE results mostly from the vertical component. The horizontal component of this energy process changes slightly or decreases during warm ENSO

years. It is worth noting that the vertical component of this energy process is excluded in the two-dimension EAPE equation used by Lau and Lau (1992) and Maloney and Dickinson (2003). Eddy vertical heat transport may play an important role in the maintenance of EAPE over the tropical WNP during warm years.

6. Summary for Part I

ENSO has been suggested as an important mechanism responsible for the interannual variability in TS activity over the WNP by modulating the large-scale environments in which the tropical storms are formed and develop (e.g. Wang and Chan 2002; Chia and Ropelewski 2002; Camargo and Sobel 2005). This implies that the relationship between ENSO and TS involves interactions among ENSO, large-scale circulation and TS that are complicated and not fully addressed. This study explored this issue through the three-dimensional primitive equation (PE) form of eddy kinetic and available potential energy diagnostics. The classification of warm and cold ENSO years in this study for composite analysis was based on the July-September averaged SST anomaly in the Niño3.4 region (Wang and Chan 2002). Consistent with previous studies (e.g. Chen et al. 1998; Chia and Ropelewski 2002; Wang and Chan 2002), the tropical storm formation region extends southeastward accompanied by southeastward extension and intensification of the monsoon trough and westerly jet during warm ENSO years. Meanwhile, the TSs are stronger and have longer life spans, which lead to the increase of accumulated cyclone energy (ACE) during warm years, as previously reported by Camargo and Sobel (2005).

From the energy point of view, the intensification and eastward extension of the westerly jet and monsoon trough during warm ENSO years establish a favorable environment for eddy barotropic conversion at low levels and eddy baroclinic energy conversion at upper levels between the Philippine Sea (130°-150°E) and the date line. Thus, the EKE increases over the region of vigorous TS activity from the Philippine Sea (130°-150°E) to the date line during warm years. Figure 6.1 illustrates the mechanisms responsible for the growth of EKE over the WNP during both the TS

formation and westward propagating stages (Fig. 6.1a) and the northward propagating stage (Fig. 6.1b). During warm ENSO years, an anomalous low-level cyclonic flow to the northwest of warm SST anomalies and the anomalous westerly jet, which is associated with anomalous Walker circulation, extend from the Philippine Sea (130°-150°E) to the central Pacific (Fig. 6.1a). Such large-scale environments with enhanced mean zonal wind convergence ($\frac{\partial \bar{u}}{\partial x}$<0) and cyclonic shears ($\frac{\partial \bar{u}}{\partial y}$<0) are favorable for the two barotropic energy conversion processes $-\overline{u'^2}\frac{\partial \bar{u}}{\partial x}$ and $-\overline{u'v'}\frac{\partial \bar{u}}{\partial y}$ during warm years. Thus, these two eddy barotropic processes significantly increase during both the TS formation and early-development stages. The increase in the former over the TS formation region supports the wave accumulation mechanism (Sobel and Bretherton 1999; Kuo et al. 2001; Tam and Li 2006).

The anomalous cyclonic circulation and westerly jet associated with the warm ENSO are also beneficial for the eastward extension of large-scale upward motion and establishment of tropical convection to the north of the westerly jet from the Philippine Sea (130°-150°E) to the date line (Fig. 6.1a). Thus, positive eddy baroclinic energy conversion from EAPE to EKE appears from the Philippine Sea (130°-150°E) to the date line during warm years. The largest eddy baroclinic energy conversion occurs at the upper levels, which is consistent with the study of Lau and Lau (1992). This result indicates that eddy baroclinic energy conversion is mostly supplied by the latent heat release associated with cumulus convection in the WNP and central Pacific regions (Lau and Lau 1992; Maloney and Dickinson 2003).

As transient eddies propagate to 130°-140°E (Fig. 6.1b), they start to propagate northward, and encounter anomalous anticyclonic circulation and descending motion

in the subtropical and mid-latitude regions (Fig. 6.1b). Transient eddies lose eddy kinetic energy to mean flow. Such large-scale environments in the subtropical and mid-latitude regions are unfavorable for the subsequent development of tropical storms (Fig. 6.1b). The subsequent development and intensification of tropical storms are mainly attributed to the enhanced eddy baroclinic energy conversion through eddy ascending motion in warm regions and descending motion in cold regions as they propagate northward into subtropical and mid-latitude regions, consistent with the results of Kung (1977). It is suggested that the baroclinic effects play an important role in TS intensity during the late stages of development, which is in support of the hypothesis of Emanuel et al. (2004).

Once EAPE is converted to EKE, the loss of EAPE due to conversion is mainly replenished by the generation of EAPE through the condensation heating associated with eddy convection. These results are similar to the findings of Lau and Lau (1992) and Maloney and Dickinson (2003) who used a two-dimensional EAPE budget equation. However, the magnitude of energy conversion from MAPE to EAPE is comparable to the EAPE generation through a three-dimensional EAPE budget equation in this study; despite that the horizontal mean temperature gradient in the tropics is small. The MAPE to EAPE energy conversion process is mainly contributed by its vertical component associated with eddy vertical heat transport. These results suggest that the eddy vertical heat transport, which is neglected in the two-dimensional EAPE budget equation (Lau and Lau 1992; Maloney and Dickinson 2003), plays an essential role in the maintenance of EAPE over the tropical storm formation and development regions.

The anomalous large-scale circulations and corresponding eddy barotropic

energy conversion modulated by ENSO events may explain the coincidence of the eastward displacement of the monsoon trough, westerly jet and TS formation region (e.g. Chen et al. 1998; Chia and Ropelewski 2002; Wang and Chan 2002; Chen et al. 2006). However, the subsequent development and intensification of transient eddies, particularly as they propagate northward into subtropical and mid-latitude regions, are mainly attributed to the enhanced eddy baroclinic energy conversion. It is suggested that tropical transient eddies including tropical storms may be self-developing and intensify through both their latent heat release and vertical heat transport, supporting the results by Ge et al. (2008). Using a baroclinic PE model, Ge et al. (2008) indicated that diabatic heating would maintain the upper level outflow jet of a TC, which may in turn influence the TC intensity and size through downward energy dispersions.

Heating associated with transient eddies over warmer regions directly induces cyclonic vorticity and westerlies at low levels and indirectly increases the baroclinicity (temperature gradient) which in turn may enhance both the low-level convergence and TS intensity. This positive feedback between conversion and circulation continuously provides energy for the development of transient eddies. The accumulation of cyclonic vorticity and westerly produced by tropical transient eddies including tropical storms may in turn alter the large-scale cyclonic circulation and ENSO (Sobel and Camargo 2005). On the other hand, the heavy precipitation and induced strong wind stress associated with transient eddies including TSs may reduce SST (e.g. Bender and Ginis 2000; Lin et al. 2003). Simultaneous occurrence of the ENSO-related anomalous SST, large-scale circulations and eddy energy processes (Fig. 6.1) causes that it's more difficult to clarify the active and passive roles among

them through the current observational study alone. To explore this issue, further investigation of the active and passive roles among anomalous SST, large-scale circulation and tropical storms through numerical experiments will be presented as the Part II of this study.

ENSO and Eddy Energetics along the Tropical Storm Track

Part II : Numerical Experiments

7. Introduction for Part II

Despite many studies suggested that the ENSO may impact on the interannual variability of TS activity over the WNP through the modulation of large-scale circulations (e.g. Wang and Chan 2002), as discussed in Part I of this study; there are other mechanisms except for ENSO may induce the interannual variations of large-scale environments.

Hsu and Liu (2003) mentioned the heating over the Tibetan Plateau would modulate the evolution and location of monsoon trough and subtropical high. During the years when the Tibetan heating weakens, the monsoon trough (subtropical high) over the WNP is strengthened (weakened). Hsu et al. (2005) pointed out the positive feedback between 30-60 day oscillation and monsoon mean flow circulation during different ENSO phases. During warm ENSO events, the 30-60 day westerly, southerly and cyclonic vorticity all enhance and extend southeastward which would contribute to the development and intensification of monsoon trough and large-scale convergence over the southeastern region of WNP.

Tropical storms themselves may influence the large-scale atmospheric and oceanic environments over the WNP to initiate the ENSO events (e.g. Keen 1982; Gao et al. 1988; Kindle and Phoebus 1995; Sobel and Camargo 2005). Keen (1982) and Kindle and Phoebus (1995) indicated that the westerly wind, which is an essential part of the establishment of El Niño, may induced by tropical cyclones when they occur near the equator. Gao et al. (1988) found that the near-equatorial cyclones would intensify equatorial westerlies and eastward-propagated Kelvin wave, inducing SST to rise over the South American coasts. Recently, Sobel and Camargo (2005)

suggested that the possibility of a two way interaction between tropical cyclone activity and ENSO event. In other words, the tropical cyclone over the WNP may contribute to the modulation of their large-scale environments. The linkage between ENSO, large-scale environments and TS activity over the WNP is still uncertain.

From the analysis of observations, the anomalous warm SST over the central-eastern Pacific, southeastward extension of monsoon trough and strong westerly all occur simultaneously. It is more difficult to clarify the active and inactive role among ENSO, large-scale circulation and TS activity through data analysis alone. A general circulation model (GCM) with the capability of performing the interannual variations of large-scale circulation as well as the tropical storm activity would be a practical tool to investigate this issue. In the past, many modeling studies have documented the atmospheric responses of Asian monsoon circulations to the different SST conditions. These representative works in 1990's have been summarized by Lau and Nath (2000). Because of the improvement of computational efficiency, many numerical experiments run with larger duration or ensembles were conducted in recent years. Following Lau and Nath (2000), some recent modeling works associated interannual variations of Asian monsoon flows were listed in Table 2. As compared with the performance of previous results, the performances of interannual variations of large-scale flows in these higher resolution or air-sea coupled GCM (CGCM) were more realistic (e.g. Fu et al. 2002; May 2003; Kucharski et al. 2007). The physical mechanisms associated with ENSO-Asian monsoon interaction were also addressed more precisely (e.g. Lau and Nath 2003; Chou 2004; Li et al. 2007).

On the other hand, some studies chose atmospheric dynamic and thermodynamic variables to be the selection criteria and developed the objective algorithm for

identifying and tracking of tropical storms in AGCM (e.g. Bengtsson et al. 1995; Vitart et al. 1997; Camargo and Zebiak 2002) although the realistic and detailed structures of typhoon are difficult to be simulated because of the coarse resolution of AGCM (Bengtsson et al. 2007; Knutson et al. 2007). Thus, the ECHAM4.6 high resolution T106 model which has the capability of simulating the interannual variations of large-scale circulations (May 2003) and tropical cyclones activity except intensity (Camargo et al. 2005), is adopted in this study to examine the interaction among SST anomalies over the tropical Pacific, large-scale circulation and TS activity over the WNP. Section 8 contains the model description, experimental designs and the TS identification in model. The role of SST anomalies over the tropical Pacific in modulating the interaction between large-scale mean flow and eddy is discussed in section 9. The summary of principle findings for numerical experiments will be shown in section 10.

8. Model description, experiments and TS identification

8.1 ECHAM4 T106 AGCM

The high-resolution atmospheric general circulation model (AGCM) used in this study is the 4.6 version of ECHAM4, which was developed at the Max-Plank-Institute for Meteorology. The detailed descriptions of ECHAM4 parameterization have been documented in Roeckner et al. (1996). This is a spectral model and has been run at spectral resolution of triangular truncation 106 (approximately 1.125º×1.125º in zonal and meridional directions) with 19 vertical levels at sigma coordinate (T106L19).

8.2 Experimental design

Three numerical experiments are designed to clarify whether ENSO-related SST anomaly plays an active role to the interannual variations of large-scale circulation and TS activity. As shown in Table 3 and Figure 8.1, each experimental design corresponds to different SST conditions.

The control experiment (CTL) is forced by the globally observed SST, which vary from years to years, for the period 1979-1999, similar to the Atmospheric Model Intercomparison Project (AMIP). This experiment would assess the model performances of interannual variations of large-scale circulations and energetic processes associated with global SSTA (Fig. 8.1a). Also, results from the CTL experiment will be applied as a reference for other experiments which change regional SST conditions.

In the second numerical experiment, named the noTPO (no tropical Pacific Ocean), the SST variations over the tropical Pacific Ocean (100ºE-80ºW, 15ºS-15ºN) are forced by climatology. Hence, the interannual variations of lower boundary forcing in the tropical Pacific basin are eliminated. The typical El Niño (La Niña)-related anomalous warming (cooling) over the central-eastern Pacific and cooling (warming) over the tropical western Pacific are both absent in this noTPO experiment (Fig. 8.1b). The atmospheric responses in this simulation may result from SST forings globally except for the tropical Pacific.

The third experiment is set up for understand the impact of local SST anomalies on large-scale circulations and TS activity over the WNP. In this experiment, model is forced by observed SST everywhere except over the tropical central-eastern Pacific (170ºE-80ºW, 15ºS-15ºN) where the climatological SST is used. The lower boundary condition in this experiment shows a cold anomaly over the tropical western Pacific for warm minus cold composites to emphasize the interannual variations associated with ENSO (Fig. 8.1c). For convenience, this experiment is named the noEPO (no eastern Pacific Ocean) experiment. Note that the atmospheric responses over the WNP might be induced from not only the local SST over the western Pacific but also other ocean basins, although the influence of remote forcing outside the tropical Pacific may be smaller than the local forcing.

The simulated results of interannual variations in large-scale flow patterns and eddy energetics as well as the associated mechanisms will be discussed in the next two sections.

8.3 TS identification and tracking methodology

To identify the TS cases in AGCM, studies (e.g. Bengtsson et al. 1995; Vitart et al. 1997; Camargo and Zebiak 2002) usually chose atmospheric dynamic and thermodynamic variables to be the selection criteria and developed the objective algorithm for identifying and tracking of tropical storms (Chauvin et al. 2006). Although the intensity of TS simulated by AGCM is weaker than observation (Bengstsson et al. 1982; Vitart et al. 1997) due to the low resolution (Bender and Ginis 2000; Knutson et al. 2007) and the convection parameterization in model (Shen et al. 2006), the climatology and interannual variability of TS occurrence over global basins are well-simulated (Bengstsson et al. 1982; Vitart et al. 1997; Camargo et al. 2005; Bengtsson et al. 2007). Vitart et al. (1997) explored that the AGCM is able to reproduce a realistic interannual variations of TS frequency if it would simulate the interannual variations of large-scale circulation over ocean basins (Camargo et al. 2005; Bengtsson et al. 2007).

This study followed the objective algorithm developed by Vitart (1997, 2003) and Knutson et al. (2007), using the 850hPa vorticity, surface pressure and well-defined warm core as the selection criteria of tropical storm. Because the number of tropical cyclones at a given intensity in vorticity or in wind speed tightly depends on the model resolution (Walsh et al. 2007), these criteria for the detection and tracking of simulated TS in different models need to be adjusted. Criteria values used with T42 AGCM in Vitart (1997) and 18-km regional climate model in Knutson et al. (2007) were significantly different. Concerning our study applied to ECHAM4 AGCM with T106 resolution, we adjust the detection criteria that are mainly based on the simulated TS numbers in warm and cold years may approach that in the

observation as far as possible.

The methodology and associated criteria for identification and trajectory tropical storms are described as follow:

Tropical storms identification: At each 6-hourly time step, select all the space points exceed following thresholds as the tropical storm candidates.

1) 850hPa relative vorticity exceeds 8×10^{-5} 1/s.

2) The mean sea level pressure is a local minimum within a distance of 4˚ latitude or longitude from the vorticity center fulfills threshold 1). The pressure increases by at least 5hPa from the storm center within a radius of 5˚. The closest minimum pressure is defined as storm center.

3) The warm core structure, determined by averaged temperature fields between 300-500hPa, exists within a distance of 4˚ latitude or longitude from storm center.

Tropical storms trajectory: The following objective procedures are used to construct the tracks of tropical storm selected by previous identification step.

1) For each storm, we first check whether there are storms within 400km during the next time step.

2) If there are none, the trajectory procedure stops. If there is more than one storm within 400km, the storm which locates closest or in the northwestern region to the initial storm will be chosen to link as the same trajectory.

3) The wind speed at lowest level exceeds 15m/s and occurs at least 6 time steps, not necessarily consecutive.

9. Simulation results

9.1 Simulation results of ENSO, large-scale circulation and TS activity

The large-scale circulation, TS frequency, formation position simulated from the ECHAM4 CTL during different ENSO phases are computed and compared to those obtained from the JTWC best track data and NCEP-DOE reanalysis, respectively, to validate the model capabilities of simulating the interannual variability of the large-scale circulation and TS activity over the WNP.

Figure 9.1 depicts the interannual variations of TS frequency and large-scale circulation over the WNP simulated by the ECHAM4 T106 control experiment. The simulated monsoon trough stretches southeastward from east of Taiwan into the tropical central Pacific during warm years (Fig. 9.1a). Although the cyclonic circulation and monsoon trough are overestimated by model, they retreat westward and are confined west of 140°E during cold years (Fig. 9.1b). Compared to observation (Figs. 4.1c and f), the simulated anomalous cyclonic flow is stronger and larger while the strength of the simulated anomalous anticyclonic flow is much weaker than observation and is confined to the southeast of China and vicinity of Taiwan (Figs. 9.1c and f). This might result from the overestimate (underestimate) the response of heating (cooling) effect in the ECHAM4 T106 model simulation.

The interannual variations of TS frequency over the WNP simulated by ECHAM4 CTL experiment (Figs. 9.1a and b) are similar to the observation (Figs. 4.1a and b), although the patterns of TS frequency in model exist eastward biases. Camargo and Sobel (2004) and Camargo et al. (2005) also found an eastward bias of cyclogenesis region over the western Pacific in ECHAM3 and ECHAM4 AGCMs

with T42 resolution. Accompanied by the eastward extension of monsoon trough and convergence region in the CTL simulations during warm years, most tropical storms are formed from the tropical central Pacific where the westerly and easterly converges (Fig. 9.1d). Then, these simulated TSs develop along the axis of monsoon trough as well as the southeasterly prevailing regions (Figs. 9.1a and d).

The linkage between ENSO-related anomalous large-scale circulation and TS activity are well-represented in the ECHAM4 CTL experiment (Fig. 9.1c). The regions where the warm anomalous SST, low-level westerly jet and strengthened cyclonic flow occur are coincident with positive anomalous TS frequency (Figs. 9.1c and f). It is suggested that the interannual variations of TS frequency and formation region between warm and cold ENSO events are closely related to the interannual variation of the large-scale circulation modulated by ENSO in the ECHAM4 CTL experiment, as in observation. These results are similar to the study of Vitart et al. (1999). They suggested that the AGCM has the ability to simulate a realistic interannual variability of TS frequency if it simulates a realistic large-scale circulation over the ocean basins.

It is noted that not only the simulated geographic distribution of TS frequency but also the simulated TS number and ACE over the WNP are similar to the interannual variations of observed TS activity indices. The simulated TS number and ACE of the CTL experiment increase during warm ENSO events (Table 4). The interannual variability (the ratio of TS number) in model is larger than that in the JTWC best-track data. Because the TS number of warm years simulated by the CTL experiment is the same as that of observation, the bias of larger ratio results from the small TS number during cold years in the model control experiment. This large ratio

of TS number in the CTL experiment might be related to a stronger interannual variation of simulated large-scale circulations. The ECHAM4 T106 control experiment tends to overestimate the strengths of anomalous cyclone, westerly jet and ascending motion over the TS formation and development regions (Fig. 9.1f). However, the intensity of simulated TS is much weaker than observation. The interannual variability of maximum wind speed and life span of TS are small (Table 4). This discrepancy suggests that AGCM with high resolution T106 still has a limited capability in simulating the TS intensity (Bengtsson et al. 2007; Knutson et al. 2007). Thus, the ration and value of ACE during warm years in the CTL experiment are both smaller than that of observation.

The interannual variations of large-scale circulations and the gross features of TS characteristics except TS intensity in the CTL experiment are similar to observation. In the following sections, we will further examine the simulated results in three numerical experiments to explore the linkage among tropical Pacific SST anomalies, the mean circulations and the TS activities over the WNP.

9.2 Impacts of tropical Pacific SST anomalies

9.2.1 Interannual variations of large-scale circulation and TS activity

As described in section 8, three experiments with different boundary conditions are conducted to clarify the relationship among ENSO, large-scale circulation and TS activity. The warm minus cold composites of SST (Fig. 8.1) and associated variables are computed respectively for the CTL, noTPO and noEPO experiments. In order to realize the contributions of anomalous forcings to atmospheric anomalies more

efficiently, the warm-minus-cold composites for CTL as well as the difference charts by subtracted simulated warm-minus-cold composites of noTPO and noEPO from that of CTL are presented in this section. As shown in Figure 9.2, the warm minus cold composites for CTL indicate the atmospheric responses to the globally anomalous SST. The contributions of combination of heating over the equatorial central-eastern Pacific and cooling over the equatorial western Pacific can be referred by taking the simulated output of CTL minus that of noTPO experiment. Similarly, the simulated results of CTL minus noEPO may be interpreted as the contributions of heating over the equatorial central-eastern warming alone to the atmospheric anomalies.

Similar to the CTL, anomalous low-level circulations associated with dipoled equatorial warm and cold SST anomalies are also characterized by a wave train structure (Fig. 9.2b). This wave train is well-organized and emanates northeastward from tropical western Pacific toward the North American (not shown), indicating the equatorial anomalous forcing and SST gradient may excite this wave train and show a teleconnection with extratropical circulation anomalies (e.g. Hoskins and Karoly 1981; Nitta 1987; Kawamura et al. 2001). However, the anticyclone anomaly (Fig. 9.2a) and low-level negative vorticity (Fig. 9.4a) located at southeast of China presented in the CTL is unapparent when the off-equatorial forcing is excluded (Figs. 9.2b and 9.4b). It implies the cold SST anomaly over the eastern coast of Asia may have some contributions to the establishment of this anticyclonic anomaly. South of the anomalous cyclone over the WNP, a strong westerly jet associated with eastward displacement of Walker circulation (Fig. 9.3b) penetrates along 0º-15ºN toward warm SST anomaly region. This strong anomalous westerly jet and cyclonic circulation induce positive vorticity which is beneficial for the large-scale ascending motion and

diabatic heating over the tropical central Pacific (Fig. 9.4b and d). The geographical distributions of increased (decreased) TS formation and frequency are coincided with the regions of anomalous cyclone (anticyclone), positive (negative) vorticity, ascending (descending) motion and diabatic heating (cooling) (Figs. 9.4b and 9.5b). These features suggest that the anomalous large-scale environments beneficial for TS formation and development over the WNP may be largely linked to the impact of equatorial ENSO-related SST anomalies rather than SST forcings in the off-equatorial Pacific as well as the SST forcings over other ocean basins.

Without the cooling effect in the equatorial western Pacific, the low-level circulation is characterized by a significant cyclonic anomaly over the WNP, which is a Rossby wave response to the anomalous heating over the equatorial central-eastern Pacific (Fig. 9.2c). Comparisons between Fig. 9.2b and 9.2c show that the low-level cyclonic anomaly and westerly jet become stronger once the cooling effect disappears. These large-scale environments over the whole WNP are favorable for the TS formation and development (Figs. 9.4c and 9.5c). It implies the warm SST anomaly tends to reinforce the development of cyclonic circulation and westerly jet, leading to an eastward-extended ascending motion of Walker circulation (Fig. 9.3c) as well as strengthened cyclonic vorticity (Fig. 9.4c), similar to the results of Wang et al. (2000) and Chou (2004). Associated with the strong westerly jet, enhanced large-scale ascending motion and diabatic heating appears along 10°N (Fig. 9.4f). Therefore, the presence of the enhanced heating may play the dominate role in setting up a favorable large-scale environments for TS formation and development. The TS formation number and ACE in the existence of equatorial heating only show maximum increases among three experiments (Table 4).

Note that the responses of the TS life spans and TS intensities to different

anomalous SST conditions are insignificant (Table 4). That is, the differences of these two indices simulated by three numerical experiments all reveal small negative values. The results are inconsistent with observation which shows prominent increases of TS life spans and intensities during warm years (Table 1).

9.2.2 Eddy energetics along the TS track

Figure 9.5 displays the EKE and TS frequency for warm minus cold composites in the CTL and the difference of associated patterns for CTL minus noTPO and noEPO experiments, respectively. The positive EKE anomalies simulated by the ECHAM4 CTL experiment appear east of 150°E where the TS frequency increase (Figs. 9.5a), while the negative EKE anomalies occur in the northwestern part of WNP where TS frequency decreases during warm years (Fig. 9.5a). These anomalous patterns are reproduced in the experiment forced by equatorial western and eastern Pacific SST anomalies (Fig. 9.5b). As the anomalous SST forcing of warming over the equatorial central-eastern Pacific is remained, the EKE and TS frequency both show larger-amplitude increases (Fig. 9.5c) than the simulated results of globally forcing run (Fig. 9.5a) and equatorial Pacific forcing run (Fig. 9.5b). Moreover, the areas of enhanced EKE and TS frequency are rather vast and prevailing over the WNP (Fig. 9.5c). These simulated results imply that the enhanced EKE associated with TS activity over the WNP is mainly connected with equatorial central-eastern Pacific SST conditions.

Figure 9.6 displays the EKE generation through barotropic and baroclinic energy conversion associated with different ENSO-related SST anomalies. Figures 9.6a and d show the simulated results of interannual variations of barotropic and baroclinic

energy conversions in the CTL experiment, respectively. Note that the anomalous positive barotropic (Fig. 9.6a) and baroclinic (Fig. 9.6d) energy conversions both dominate in the south of 20ºN over the WNP and maximize between 150ºE-180º where coincides with the enhanced EKE and TS frequency during warm years (Fig. 9.5a). The magnitudes of enhanced barotropic and baroclinic energy conversions are comparable, indicating that the increased EKE associated with active TS motions (Fig. 9.5a) are converted through both barotropic and baroclinic energy conversions. These two eddy energy conversion processes display negative anomalies in the extratropical and mid-latitude regions (Figs. 9.6a and d). This implies that the TS would gain less EKE during warm years when they propagate northward. It may lead to the inactive TS activity over the subtropical western Pacific (Fig. 9.5a).

Based on the energetic result of observation (Fig. 5.2f), the enhanced baroclinic energy conversion plays an important role in maintaining the eddy growth in the extratropical and mid-latitude regions. Contrary to the observation, the ECHAM4 CTL experiment produces less baroclinic energy conversion in the subtropical WNP during warm years (Fig. 9.6d). This discrepancy would be one reason for model to underestimate the intensity of TS during warm years. When the simulated TSs propagates northward, it may not have enough EKE supply from baroclinic energy conversion which maintains the development of TS in real atmosphere during warm years.

Changes of low boundary condition mainly affect the amplitudes of eddy barotropic energy conversion rather than the geographical distribution of it (Figs. 9.6a-c). In the absence of off-equatorial SST anomalies (Fig. 9.6b), the positive barotropic energy conversion anomaly shows somewhat increase along the TS track

as compared with CTL (Fig. 9.6a). The increase magnitude of enhanced barotropic energy conversion is more evident while retaining the warm SST forcing over the central-eastern Paciic only (Fig. 9.6c). These results suggest that the ENSO-related SST anomaly would alter the large-scale circulations and in turn influence the EKE generation through eddy barotropic energy conversion process. However, the simulated eddy baroclinic energy conversions among three numerical experiments reveal insignificant changes in both spatial pattern and magnitudes (Figs. 9.6d-f). It suggests that the anomalous SST forcings have little contribution to the strengths of eddy vertical motion and temperature associated with baroclinic energy conversion.

Since the geographical distributions of anomalous barotropic and baroclinic energy conversions are similar in three experiments, Figure 9.7 just shows the differences of vertical cross section along TS track of barotropic and baroclinic energy conversions between warm and cold years in the CTL experiment. Consistent with the observation (Fig. 5.3c), the simulated barotropic energy conversion of CTL shows positive anomalies in the low-levels during warm years (Fig. 9.7a). The region of enhanced barotropic energy conversion agrees with the eastward-extended anomalous westerly, although it has an eastward shift as compared to the observation (Fig. 5.3c). Contrary to the barotropic energy conversion, the simulated baroclinic energy conversions, associated with the covariance between vertical motion and temperature of eddies, occur in higher troposphere (Fig. 9.7b). This implies the low-level vertical motion associated with eddy disturbances is weak in the CTL experiment, since the surface heat flux associated with ENSO forcing has small contribution to the eddy baroclinic energy conversion (Figs. not shown), in agreement with the observation (Fig. 5.3f).

Barotropic energy conversion between MKE and EKE is determined by the interactions between mean flow and eddy momentum. The different responses of large-scale circulations and eddy transports associated with SST anomalous conditions would impact on barotropic energy processes. In order to realize precisely the mechanisms of barotropic energetic processes modulating by the interannual variations of tropical Pacific SST, we further compare each term of barotropic energy conversion in the model simulations. Figure 9.8 displays the vertical profiles of individual term of anomalous barotropic energy conversion over the TS formation and development region (140ºE-180º, 10º-20ºN). It is clear that the low-level positive anomalous barotropic energy conversions in the three experiments are mainly attributed by both the terms $-\overline{u'^2}\frac{\partial \bar{u}}{\partial x}$ and $-\overline{u'v'}\frac{\partial \bar{u}}{\partial y}$ (Figs. 9.8a-c). This suggests the interactions between large-scale zonal wind anomalies and horizontal eddy momentums are prominent during warm years. The term $-\overline{u'\omega'}\frac{\partial \bar{u}}{\partial p}$, associated with the interaction between vertical eddy momentum and large-scale vertical wind shear, plays a minor role in the enhancement the barotropic energy conversions during warm years. Conversion by term $-\overline{v'^2}\frac{\partial \bar{v}}{\partial y}$ shows negative anomaly in the troposphere.

Figure 9.9 shows the spatial distributions of the most leading terms in barotropic energy conversion. The major regions with enhanced $-\overline{u'^2}\frac{\partial \bar{u}}{\partial x}$ and $-\overline{u'v'}\frac{\partial \bar{u}}{\partial y}$ are coincident among three experiments except for amplitudes. The occurrence of anomalous positive barotropic conversion by $-\overline{u'^2}\frac{\partial \bar{u}}{\partial x}$ (Figs. 9.9a-c) and $-\overline{u'v'}\frac{\partial \bar{u}}{\partial y}$ (Figs. 9.9d-f) are closely linked to the anomalous low-level westerly jet and cyclonic flow associated with the warm SST anomalies over the equatorial central-eastern

Pacific. Positive anomaly of $-\overline{u'^2}\frac{\partial \bar{u}}{\partial x}$ are concentrated in the exit of strong westerly ($\frac{\partial \bar{u}}{\partial x} < 0$) along 10°-20°N (Figs. 9.9a-c). Strong EKE generation through $-\overline{u'^2}\frac{\partial \bar{u}}{\partial x}$ (Figs. 9.9a-c) is in general accompanied by wave accumulation for tropical disturbances growth. In addition, eddy momentum transport within a cyclonic shear region may contribute barotropic energy conversion of $-\overline{u'v'}\frac{\partial \bar{u}}{\partial y}$. The enhanced $-\overline{u'v'}\frac{\partial \bar{u}}{\partial y}$ appears in the cyclonic shear regions north of westerly jet (Figs. 9.9d-f). Note that the magnitudes of enhanced $-\overline{u'^2}\frac{\partial \bar{u}}{\partial x}$ and $-\overline{u'v'}\frac{\partial \bar{u}}{\partial y}$ are both increased accompanied by the enhanced strength of westerly jet and anomalous cyclonic circulations.

Therefore, tropical SST anomalies could modulate the large-scale flow patterns and then affect the interaction between mean flows and eddies through barotropic energy conversion. The ENSO-related warm SST anomaly over the central-eastern Pacific induces strong westerly and cyclonic anomalies that are accompanied with the enhancement of zonal convergence and cyclonic wind shear, producing favorable environments for barotropic energy conversion and wave accumulation. Thus, increased genesis number, frequency and vigorous motion of tropical storms are detected over the WNP during ENSO warm events.

Through the diagnosis of the energy conversion between MAPE and EAPE and the EAPE generation by diabatic heating, we further examine the mechanisms responsible for the supplement of EAPE which converts to EKE along the TS track. The geographical distributions of these two energy processes are represented in Figure 9.10. The simulated baroclinic energy conversion is maintained by the EAPE generation. In the three numerical experiments, the horizontal distributions of

anomalous EAPE generation (Figs. 9.10d-f) resemble with those of baroclinic energy conversion from EAPE to EKE (Figs. 9.6d-f). Simulated results of the numerical experiments indicate that the EAPE consumed by enhanced baroclinic energy conversion is compensated by the generation of EAPE associated with diabatic heating, which is agreement with observation.

The latent heat release by eddy itself would generate EAPE and then convert to EKE for the growth of eddy disturbances (Lau and Lau 1992; Maloney and Dickinson 2003; Hsieh and Cook 2007). In other word, once the TS initiates and excites strong ascending convection, the latent heat release of eddy disturbance might self-sustain its strength through eddy baroclinic energy conversion. In this way, a precise estimation of convective heating would act as a crucial role to determine the TS intensity in model simulations. The underestimation of TS intensity in the ECHAM4 CTL experiment might be partly due to the simulated biases of EAPE generation and baroclinic energy conversions during TS development stages.

Another possible reason to underestimate the TS intensity in model might arise from the insufficient MAPE to EAPE conversion for maintaining the enhanced baroclinic energy conversion during warm years. Along the TS track, not only the spatial distribution (Figs. 9.10a-c) but also vertical profiles (not shown) of MAPE to EAPE conversion anomalies simulated by ECHAM4 are insignificant. These simulated results in the CTL experiment are inconsistent with observation (Fig. 5.5c) which shows the enhanced MAPE to EAPE conversion is one of the important energetics processes maintaining the enhanced EPAE to EKE conversion during warm years. Through the strengthened vertical eddy heat transport in the regions with mean vertical temperature gradient, the EAPE is converted from MAPE in

observation (Fig. 9.11b). However, the vertical component of MAPE to EAPE conversion is as weak as its horizontal component in the ECHAM4 CTL experiment (Figs. 9.11c and d).

We further examine the associated variables of this energy conversion process (C_A in equation (4)). It is found that the eddy thermal advection as well as mean temperature gradient has significant increase during warm years in ECHAM4 model (Figs. not shown). The underestimates of MAPE to EAPE conversion is mainly due to the small differences of simulated static stability between warm and cold years. In other word, the responses of atmospheric static stability to SST anomalies in ECHAM4 are too small to produce an enhanced MAPE to EAPE conversion in model simulation during warm years.

10. Summary for Part II

Numerical experiments using ECHAM4 T106 AGCM are performed to understand the relationship between the tropical Pacific SST anomalies associated with ENSO, large-scale circulations and tropical storm. Three different SST conditions are used as the lower boundary forcing of the AGCM throughout the 1979-1999 period. The control experiment (CTL) is forced globally by the observed monthly SST with interannual variability. The noTPO experiment is forced by the observed SST everywhere except over the tropical Pacific (100°E-80°W, 15°S-15°N) where the climatological SST is used, in order to eliminate the equatorial (15°S-15°N) ENSO-related western-eastern Pacific dipole SST forcing. In the noEPO experiment, the climatological SST is used over the tropical eastern Pacific (170°E-80°W, 15°S-15°N) while the observed SST is used in all remaining ocean as the forcing. Thus, difference between CTL and noTPO (warm-minus-cold composites of the former minus those of the latter) may be inferred as the contributions of warming over the equatorial central-eastern Pacific and cooling over the equatorial western Pacific. In analogy, the results of CTL minus noEPO represent the warming effect over the equatorial central-eastern Pacific alone.

The ECHAM4 T106 AGCM has the capability of reproducing the changes of large-scale circulation over the WNP modulated by the ENSO-related SST anomalies during warm years, although this model tends to overestimate the cyclonic circulation and monsoon trough associated with the warm SST forcing over the WNP during cold years. The regions with anomalous cyclonic circulation, ascending motion and low-level westerly jet coincide with the anomalous high TS frequency in the CTL experiment, as in observation. This result is consistent with Vitart et al. (1999) who

mentioned that the simulated interannual variations of TS frequency are significantly connected to the simulated large-scale circulations over the ocean basins. Such large-scale circulations lead to the enhancement of barotropic and baroclinic energy conversions that are responsible for the southeastward displacement of TS genesis region to the central Pacific, consistent with the results of observation.

The simulated results of three numerical experiments may explain the relative contributions of equatorial Pacific SST anomalies to the large-scale circulation and the activity of transient eddies including tropical storms. On condition that the warming forcing over the equatorial central-eastern Pacific exists, the large-scale flow patterns beneficial for the TS formation and development are well reproduced, as shown in CTL forced by globally SST anomalies. The atmospheric responses to the combination of heating in equatorial central-eastern Pacific and cooling in the equatorial western Pacific are similar to that forced by the heating over the central-eastern Pacific alone, except for the amplitudes of associated anomalous circulations. The spatial scales and magnitudes of cyclonic anomaly, strong westerly, enhanced ascending motion and diabatic heating over the WNP in the former is smaller and weaker than that in the latter. It implies that the heating effect is the essential contributors to establish the favorable environments for TS formation and development. While the cooling effect in the equatorial and extratropical western Pacific would be connected to the appearance of anticyclonic anomaly over the East Asia. This anomalous anticyclone may partially counteract the atmospheric signals induced by the warm SST anomaly over the central-eastern Pacific.

Based on the examination and comparison of three numerical simulation results, we would suggest that the ENSO-related SST anomalies over the tropical Pacific act

as the dominant role in the interannual variations of TS formation region and frequency through modulating the large-scale circulations as well as the eddy energy processes over the WNP. However, the interannual variation of TS life span and TS intensity simulated by ECHAM4 T106 is small. The energetic results of the CTL simulation reveal that the enhanced eddy barotropic and baroclinic energy conversions for warm-minus-cold composites are weaker than that of observation. These biases are resulted from the inadequate simulation of ECHAN4 during cold years since the simulated results during warm years show the resemblances as compared with observation. ECHAM4 tends to overestimate of anomalous diabatic heating and eddy baroclinic energy conversion as well as overestimate the intensity of monsoon trough and barotropic energy conversion during cold years. These simulated results would lead to the deterioration of TS life span and intensity simulation during cold years and cause insignificant interannual variations of the life span and intensity of TS. The inadequate simulation of monsoon trough during cold years might be related to the overestimated anomalous cyclonic circulation associated with the warm SST forcing over the WNP and the overestimated the intensity of transient eddies including TSs during cold years. Air-sea feedback from large-scale circulation has been noted by many studies (e.g. Wang et al. 2000; Fu et al. 2002; Lau and Nath 2006). It is suggested that the transient eddies including TSs may also modulate the large-scale circulation and oceanic environments (e.g. Bender and Ginis, 2000; Lin et al. 2003) and then in turn influence the TS track and life span.

The ECHAM4 T106 significantly underestimates the intensity of TS during both warm and cold ENSO years as compared with the JTWC best track data. The insufficient resolution of ECHAM4 T106 (~100km) may be one reason accounting

for the underestimation of TS intensity. Bengtsson et al. (2007) and Knutson et al. (2007) suggested that high-resolution models with 10-20 km grid spacing may have the ability to represent the structures and strength of hurricane. These discrepancies would reduce the intensity of transient eddy including TS through self development process and in turn the interaction between transient eddies and large-scale circulation in model. A higher resolution model and/or air-sea coupled model might improve the TS intensity and track simulation.

Reference

Annamalai, H., K. Hamilton, and K.R. Sperber, 2007: The South Asian Summer Monsoon and Its Relationship with ENSO in the IPCC AR4 Simulations. *J. Climate*, **20**, 1071–1092.

Ashok, K., Z. Guan, N.H. Saji, and T. Yamagata, 2004: Individual and Combined Influences of ENSO and the Indian Ocean Dipole on the Indian Summer Monsoon. *J. Climate*, **17**, 3141–3155.

Behera, S.K., J.J. Luo, S. Masson, S.A. Rao, H. Sakuma, and T. Yamagata, 2006: A CGCM Study on the Interaction between IOD and ENSO. *J. Climate*, **19**, 1688–1705.

Bell G. D., Coauthors, 2000: Climate assessment for 1999. *Bull. Am. Meteorol. Soc.*, **81**, S1–S50.

Bender, M. A., and I. Ginis, 2000: Real-case simulations of hurricane-ocean interaction using a high-resolution coupled model: Effects on hurricane intensity. *Mon. Wea. Rev.,* **128,** 917-946.

Bengtsson L., H. Böttger, and M. Kanamitsu, 1982: Simulation of hurricane-type vortices in a general circulation model. *Tellus*, **34**, 440-457.

------, M. Botzet and M. Esch, 1995: Hurricane-type vortices in a general circulation model. *Tellus*, **47A**, 175-196.

------, K. I. Hodges, M. Esch, 2007: Tropical cyclones in a T159 resolution global climate model: comparison with observations and re-analyses. *Tellus*, **59A**, 396-416.

Camargo S. J, Stephen E. Zebiak, 2002: Improving the detection and tracking of tropical cyclones in atmospheric general circulation models. *Wea. Forecasting*, **17**, 1152-1162.

------, and Adam H. Sobel, 2004: Formation of tropical storms in an atmospheric general circulation model. *Tellus*, **56A**, 56-67.

-----, Anthony G. Barnston, and Stephen E. Zebiak, 2005: A statistical assessment of tropical cyclone activity in atmospheric general circulation models. *Tellus*, **57A**, 589-604.

------, and A.H. Sobel, 2005: Western North Pacific tropical cyclone intensity and ENSO. *J. Climate*, **18**, 2996–3006.

Chan, Johnny C. L., and K. S. Liu, 2004: Global warming and western North Pacific typhoon activity from an observational perspective. *J. Climate*, **17**, 4590-4602.

------, 2005: Interannual and interdecadal variations of tropical cyclone activity over the western North Pacific. *Meteorol. Atmos. Phys.*, **89**, 143-152.

Chauvin, F., J.-F. Royer and M. Déque, 2006: Response of hurricane-type vortices to global warming as simulated by ARPEGE-Climat at high resolution, *Clim. Dynamics*, **27**, 377–399.

Chen, T.-C., S.-P. Weng, N. Yamazaki, and S. Kiehne, 1998: Interannual variation in the tropical cyclone formation over the western North Pacific. *Mon. Wea. Rev.,* **126,** 1080-1090.

------, S.Y. Wang, and M.C. Yen, 2006: Interannual variation of the tropical cyclone activity over the western North Pacific. *J. Climate*, **19**, 5709–5720.

Chia H. H and C. F. Ropelewski, 2002: The interannual variability in the genesis location of tropical cyclones in the Northwest Pacific. *J. Climate,* **15**, 2934-2944.

Chou, C., 2004: Establishment of the low-level wind anomalies over the western North Pacific during ENSO development. *J. Climate*, **17**, 2195-2212.

Emanuel, K., C. DesAutels, C. Holloway, and R. Korty, 2004: Environmental control of tropical cyclone intensity. *J. Atmos. Sci.*, **61**, 843-858.

Fu, X., B. Wang, and T. Li, 2002: Impacts of air–sea coupling on the simulation of mean Asian summer monsoon in the ECHAM4 model. *Mon. Wea. Rev.*, **130**, 2889-2904.

Gao S., J. Wang, and Y. Ding, 1988: The triggering effect of near-equatorial cyclones on El Niño. *Adv. Atmos. Sci.*, **5**, 87-95.

Ge, X., T. Li, Y. Wang, and M.S. Peng, 2008: Tropical Cyclone Energy Dispersion in a Three-Dimensional Primitive Equation Model: Upper-Tropospheric Influence. *J. Atmos. Sci.*, **65**, 2272–2289.

Gill, A. E., 1980: Some simple solutions for heat induced tropical circulation. *Quart. J. Roy. Meteor. Soc.,* **106,** 447–462.

Gray W. M., 1979: Hurricanes: Their formation, structure and likely role in the general circulation. *Meteorology over the Tropical Oceans,* D. B. Shaw, Ed., Royal Meteorological Society, 155-218.

Holland, G. J., 1995: Scale interaction in the western Pacific monsoon. *Meteor. Atmos. Phys.,* **56,** 52–79.

Hoskins, B.J., and D.J. Karoly, 1981: The Steady Linear Response of a Spherical Atmosphere to Thermal and Orographic Forcing. *J. Atmos. Sci.*, **38**, 1179–1196.

Hsieh J.-H. and K. H. Cook, 2007: A study of the energetics of African easterly waves using a regional climate model. *J. Atmos. Sci.*, **64**, 421-440.

Hsu, H.-H., and X. Liu, 2003: Relationship between the Tibetan Plateau heating and East Asian summer monsoon rainfall. *Geophys. Res. Lett*, **30**, 2066-2069.

Hsu, Pang-chi, Tsou, C.-H., W.-S. Kau, H.-H. Hsu, 2005: Interannual variations of the intraseasonal oscillation during typhoon season over western Pacific. *Atmosphere Science*, **33**, 29-48. (in Chinese with an English abstract)

Hu Q., Y. Tawaye, and S. Feng, 2004: Variations of the northern hemisphere atmospheric energetics: 1948–2000, *J. Climate,* **17**, 1975-1986.

JTWC, cited 2008: Joint Typhoon Warning Center best track data site. [Available online at https://metocph.nmci.navy.mil/jtwc.php].

Kanamitsu, M., Ebisuzaki, W., Woollen, J., Yang, S.-K., Hnilo, J. J., Fiorino, M. and Potter, G. L., 2002: NCEP-DOE AMIP-II reanalysis (R-2). *Bull. Am.*

Meteorol. Soc., **83**, 1631-1643.

Kawamura R., T. Matsuura, and I. Satoshi, 2001b: Interannual atmosphere–ocean variations in the tropical western North Pacific relevant to the Asian summer monsoon–ENSO coupling. *J. Meteor. Soc. Japan*, **79**, 883–898.

Keen R. A., 1982: The role of cross-equatorial tropical cyclone pairs in the Southern Oscillation. *Mon. Wea. Rev.*, **110**, 1405–1416.

Kindle J. C., and P. A. Phoebus, 1995: The ocean response to operational westerly wind bursts during the 1991-1992 El Niño. *J. Geophys. Res.*, **100**, 4893-4920.

Knutson, T. R., Joseph J. Sirutis, Stephen T. Garner, Isaac M. Held, and Robert E. Tuleya, 2007: Simulation of the recent multidecadal increase of Atlantic hurricane activity using an 18-km-grid regional model. *Bull. Am. Meteorol. Soc.*, **88**, 1549-1565.

Kucharski, F., A. Bracco, J.H. Yoo, and F. Molteni, 2007: Low-Frequency Variability of the Indian Monsoon–ENSO Relationship and the Tropical Atlantic: The "Weakening" of the 1980s and 1990s. *J. Climate*, **20**, 4255–4266.

Kung, E. C., 1966: Kinetic energy generation and dissipation in the large-scale atmospheric circulation. *Mon. Wea. Rev.,* **94,** 67-82.

------, 1977: Energy sources in middle-latitude synoptic-scale disturbances. *J. Atmos. Sci.*, **34**, 1352-1365.

Kuo, H.C., J.H. Chen, R.T. Williams, and C.P. Chang, 2001: Rossby waves in zonally opposing mean flow: Behavior in Northwest Pacific summer monsoon. *J. Atmos. Sci.*, **58**, 1035–1050.

Landsea, C. W., 2000: El Nino–Southern Oscillation and the seasonal predictability of tropical cyclones. *El Nino: Impacts of Multiscale Variability on Natural Ecosystems and Society,* H. F. Diaz and V. Markgraf, Eds., Cambridge University Press, 149-181.

Lau, K.-H., and N.-C. Lau, 1992: The energetics and propagation dynamics of tropical summertime synoptic-scale disturbances. *Mon. Wea. Rev.,* **120,**

2523-2539.

Lau N.-C., and M. J. Nath, 2000: Impact of ENSO on the variability of the Asian–Australian monsoons as simulated in GCM experiments. *J. Climate*, **13**, 4287–4309.

------, and ------, 2003: Atmosphere–Ocean Variations in the Indo-Pacific Sector during ENSO Episodes. *J. Climate*, **16**, 3–20.

------, and ------, 2006: ENSO modulation of the interannual and intraseasonal variability of the East Asian monsoon—A model study. *J. Climate*, **19**, 4508-4530.

Li, T., 2006: Origin of the summertime synoptic-scale wave train in the western North Pacific. *J. Atmos. Sci.*, 63, 1093-1102.

Li, Y., R. Lu, and B. Dong, 2007: The ENSO–Asian Monsoon Interaction in a Coupled Ocean–Atmosphere GCM. *J. Climate*, **20**, 5164–5177.

Lin, I-I, W. T. Liu, C.-C. Wu, J. C. H. Chiang, and C.-H. Sui, 2003: Modulation of boundary layer winds by typhoon-induced upper ocean cooling, *Geophys. Res. Lett.*, **30**, 1131, doi:10.1029/2002GL015674.

Lorenz E. N., 1955: Available potential energy and the maintenance of the general circulation. *Tellus*, **7**, 157-167.

------, 1967: *The Nature and Theory of the General Circulation of the Atmosphere*. World Meteorological Organization.

Maloney, E. D., and D. L. Hartmann, 2001: The Madden–Julian Oscillation, barotropic dynamics, and North Pacific tropical cyclone formation. Part I: Observations. *J. Atmos. Sci.,* **58,** 2545-2558.

------, and M. J. Dickinson, 2003: The intraseasonal oscillation and the energetics of summertime tropical western North Pacific synoptic-scale disturbances. *J. Atmos. Sci.,* **60,** 2153-2168.

May, W., 2003: The Indian summer monsoon and its sensitivity to the mean SSTs: Simulations with the ECHAM4 AGCM at T106 horizontal resolution. *J.*

Meteor. Soc. Japan, **181**, 57-83.

McBride, J. L., 1995: Tropical cyclone formation. *Global Perspective on Tropical Cyclones,* WMO Tech Doc. 693, World Meteorological Organization, 63-105.

Nitta T., 1987: Convective activities in the tropical western Pacific and their impacts on the Northern Hemisphere summer circulation. *J. Meteor. Soc. Japan*, **65**, 373–390.

Norquist, D. C., E. E. Recker, and R. J. Reed, 1977: The energetics of African wave disturbances as observed during phase III of GATE. *Mon. Wea. Rev.,* **105,** 334-342.

Oort A. H., 1964: On estimates of the atmospheric energy cycle. *Mon. Wea. Rev.,* **92**, 483-493.

Philander, S. G. H., 1985: El Niño and La Niña. *J. Atmos. Sci.*, **42**, 2652-2662.

Reynolds, R. W. and T. M. Smith, 1994: Improved global sea surface temperature analyses. *J. Climate*, **7**, 929-948.

Ritchie, E. A., 1995: Mesoscale aspects of tropical cyclone formation. Ph.D. dissertation, Center for Dynamical Meteorology and Oceanography, Monash University, Melbourne, Australia, 167pp.

Robertson F. R. and P.J. Smith, 1983: The impact of model moist processes on the energetics of extratropical eyclones. *Mon. Wea. Rev.,* **111**, 723-744.

Roeckner E., Coauthors, 1996: The atmospheric general circulation model ECHAM4: Model description and simulation of present day climate. Max Planck Institute for Meteorology Rep. 218.

Shen, B.-W., R. Atlas, J.-D. Chern, O. Reale, S.-J. Lin, T. Lee, and J. Chang, 2006: The 0.125 degree finite-volume general circulation model on the NASA Columbia supercomputer: Preliminary simulations of mesoscale vortices. *Geophysical Research Letters,* **33**, doi:10.1029/2005GL024594.

Sobel A. H., and C. S. Bretherton, 1999: Development of synoptic-scale disturbances over the summertime tropical northwest Pacific. *J. Atmos. Sci.*, **56**,

3106-3127.

------, and S.J. Camargo, 2005: Influence of western North Pacific tropical cyclones on their large-scale environment. *J. Atmos. Sci.*, **62**, 3396-3407.

Tam, C.-Y. and T. Li, 2006: The origin and dispersion characteristics of the observed summertime synoptic-scale waves over the western Pacific. *Mon. Wea. Rev.*, **134**, 1630-1646.

Vitart F., J. L. Anderson, and W. F. Stern, 1997: Simulation of the interannual variability of tropical storm frequency in an ensemble of GCM integrations. *J. Climate*, **10**, 745-760.

------, J. L. Anderson, and W. F. Stern, 1999: Impact of large-scale circulation on tropical storm frequency, intensity, and location, simulated by an ensemble of GCM integrations. *J. Climate*, **12**, 3237-3254.

------, D. Anderson, and T. Stockdale, 2003: Seasonal forecasting of tropical cyclone landfall over Mozambique. *J. Climate,* **16,** 3932-3945.

Walsh K. J. E., M. Fiorino, C. W. Landsea, and K. L. McInnes, 2007: Objectively determined resolution-dependent threshold criteria for the detection of tropical cyclones in climate dodels and reanalyses. *J. Climate*, **20**, 2307-2314.

Wang B., R. Wu, and X. Fu, 2000: Pacific-east Asian teleconnection: How does ENSO affect East Asian climate? *J. Climate*, **13**, 1517–1536.

------, and J. C. L. Chan, 2002: How strong ENSO events affect tropical storm activity over the western North Pacific. *J. Climate.,* **15**, 1643-1658.

Yanai, M., S. Esbensen, and J. H. Chu, 1973: Determination of bulk properties of tropical cloud clusters from large-scale heat and moisture budgets. *J. Atmos. Sci.,* **30,** 611-627.

Yoo, S.H., C.H. Ho, S. Yang, H.J. Choi, and J.G. Jhun, 2004: Influences of Tropical Western and Extratropical Pacific SST on East and Southeast Asian Climate in the Summers of 1993–94. *J. Climate*, **17**, 2673–2687.

Table 1. Interannaul variations in TS number, ACE, life span and maximum wind speed for the JTWC best-track data. The numbers shown are the values of TS activity indices for warm and cold years, as well as the ratio between warm and cold years.

TS activity indices	**W**	**C**	**W/C**
Number	**54**	**49**	**1.10**
ACE (10^4 m^2/s^2)	**55.14**	**25.41**	**2.17**
Lifespan (day)	**9.75**	**6.59**	**1.48**
Max wind (m/s)	**47.57**	**37.46**	**1.27**

Table 2 Survey of modeling studies on the responses of Asian monsoon flow to the different low boundary conditions

	Model	Duration of SST forcing	Ensemble members	Domain of varying SST forcing
Fu et al. (2002)	Atmos: ECHAM4 T30L19 Ocean: WLF 2°×1°	1979-1994	1	Indian Ocean Pacific Ocean
May (2003)	Atmos: ECHAM4 T106L19	1979-1994	1	globally
Lau and Nath (2003)	Atmos: GFDL R30L14 Ocean: MLM	1950-1999	16	Tropical central-eastern Pacific
Yoo et al. (2004)	Atmos: SNU T31L20 Ocean: CCM3 slab model	1980-1994	6	tropical & extratropical Pacific
Chou (2004)	Atmos: QTCM1	10-years	1	Eastern Pacific Western Pacific Indian Ocean
Ashok et al. (2004)	Atmos: FrAM1.0 T42L18	1958-1997	5	globally
Behera et al. (2006)	Atmos: ECHAM4 T106L19 Ocean: OPA8.2 2°×0.5°	220-yr-long	1	Tropical Ocean
Kucharski et al. (2007)	Atmos: ITCP R30L8 Ocean: MOCIOM2.9 12°×1°	1950-1999	10	Indian Ocean
Li et al. (2007)	CGAM: HadCM3 2.5°×3.75°L19 (atmos) 1.25°×1.25° L20 (ocean)	1000-yrars	1	globally
Annamalai et al. (2007)	Model groups of IPCC AR4	1850-present (20c3m)	1	globally

Table 3 Numerical experiments with different regional SST

Expt	SST boundary condition
CTL	Globally observed SST
noTPO	Observed SST everywhere except tropical Pacific Ocean (170ºE-80ºW, 15ºS-15ºN)
noEPO	Observed SST everywhere except Central-Eastern Pacific (100ºE-80ºW, 15ºS-15ºN)

Table 4. The warm-minus-cold composite of TS number, ACE, maximum sustained wind speed and lifespan for the ECHAM4 T106 CTL aw well as the differences of these associated indices between CTL and noTPO / noEPO experiments, respectively.

TS activity indices	**CTL(W-C)**	**CTL (W-C) minus noTPO (W-C)**	**CTL(W-C) minus noEPO (W-C)**
Number	24	19	38
ACE (10^4 m^2/s^2)	5.3	6.04	9.85
Lifespan (day)	-0.6	-0.85	-0.6
Max wind (m/s)	-0.43	-0.17	-0.68

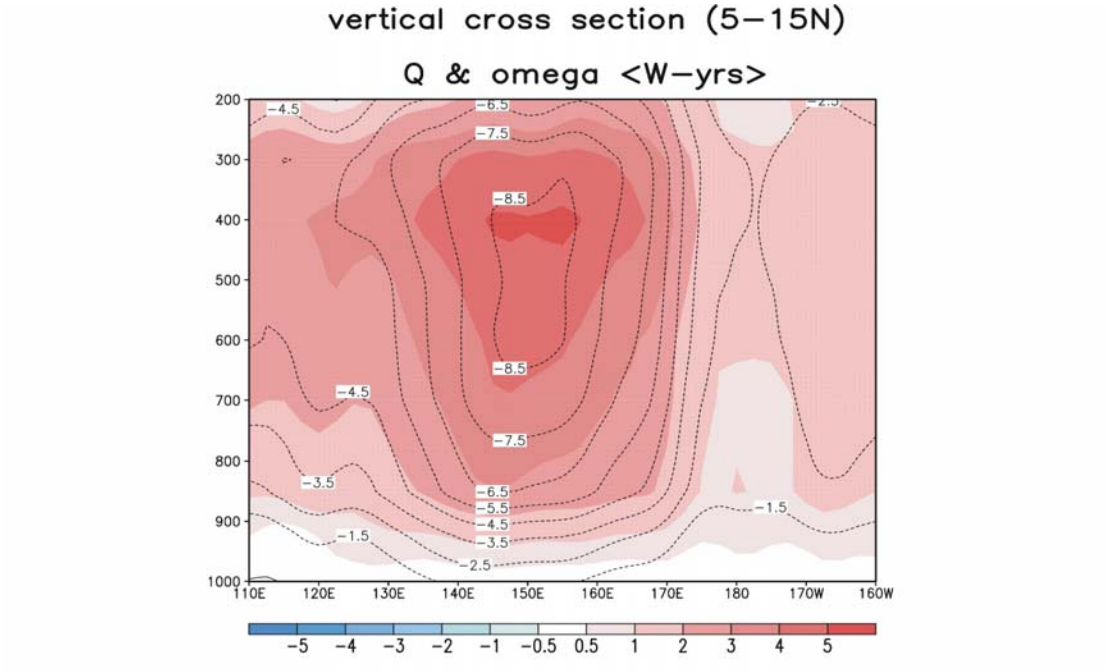

Figure 3.1 Vertical cross section of diabatic heating (10^{-5} K/s, shaded) and pressure velocity (10^{-2} Pa/s, contour) along 5°-15°N for warm composites.

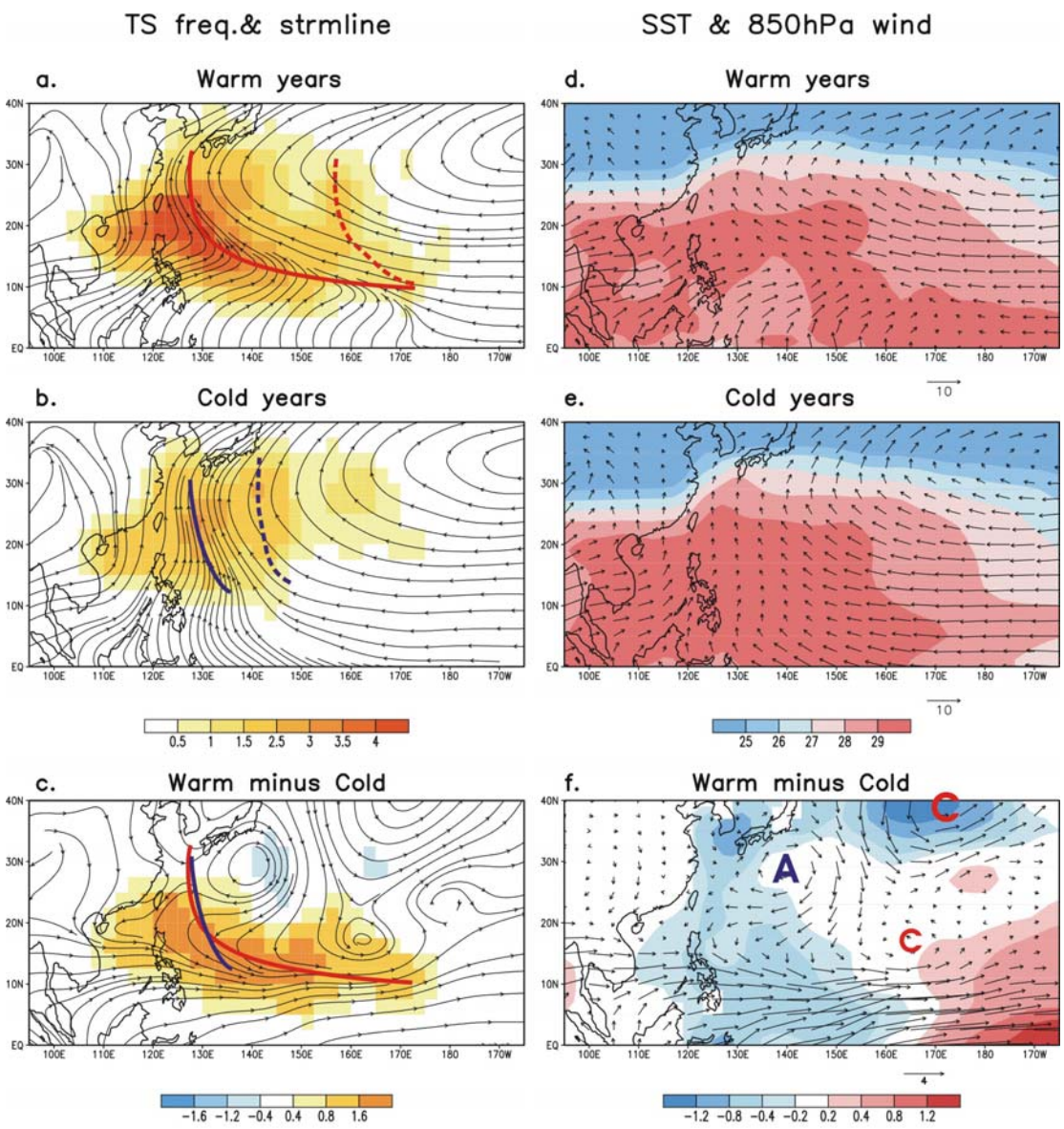

Figure 4.1 Distribution of TS frequency (shaded, unit: numbers per 2.5° longitude/latitude per JAS period) and 850 hPa streamline for (a) warm composites, (b) cold composites and (c) warm minus cold composites. (d)-(f) are same as (a)-(c), but for the July-September SST (shaded, unit: °C) and 850 hPa wind fields (vector, unit: m/s). The solid (dash) line superimposed on figures (a)-(c) represents the primary (secondary) track. Red and blue lines indicate the TS track of warm and cold years, respectively. The characters A and C in (f) represent the locations of anomalous anticyclone and cyclone, respectively.

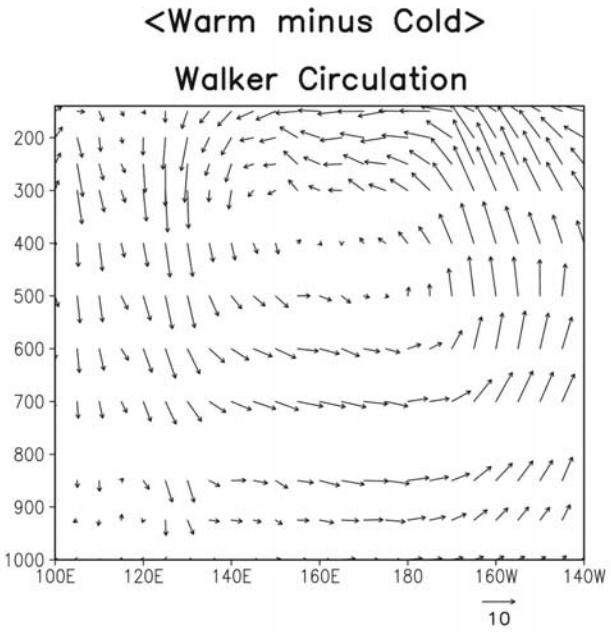

Figure 4.2 Vertical cross section of circulation along equator (averaged between 5°S-5°N) for warm minus cold composites. The scale of vertical motion (Pa/s) is multiplied by 100. The unit of zonal wind is m/s.

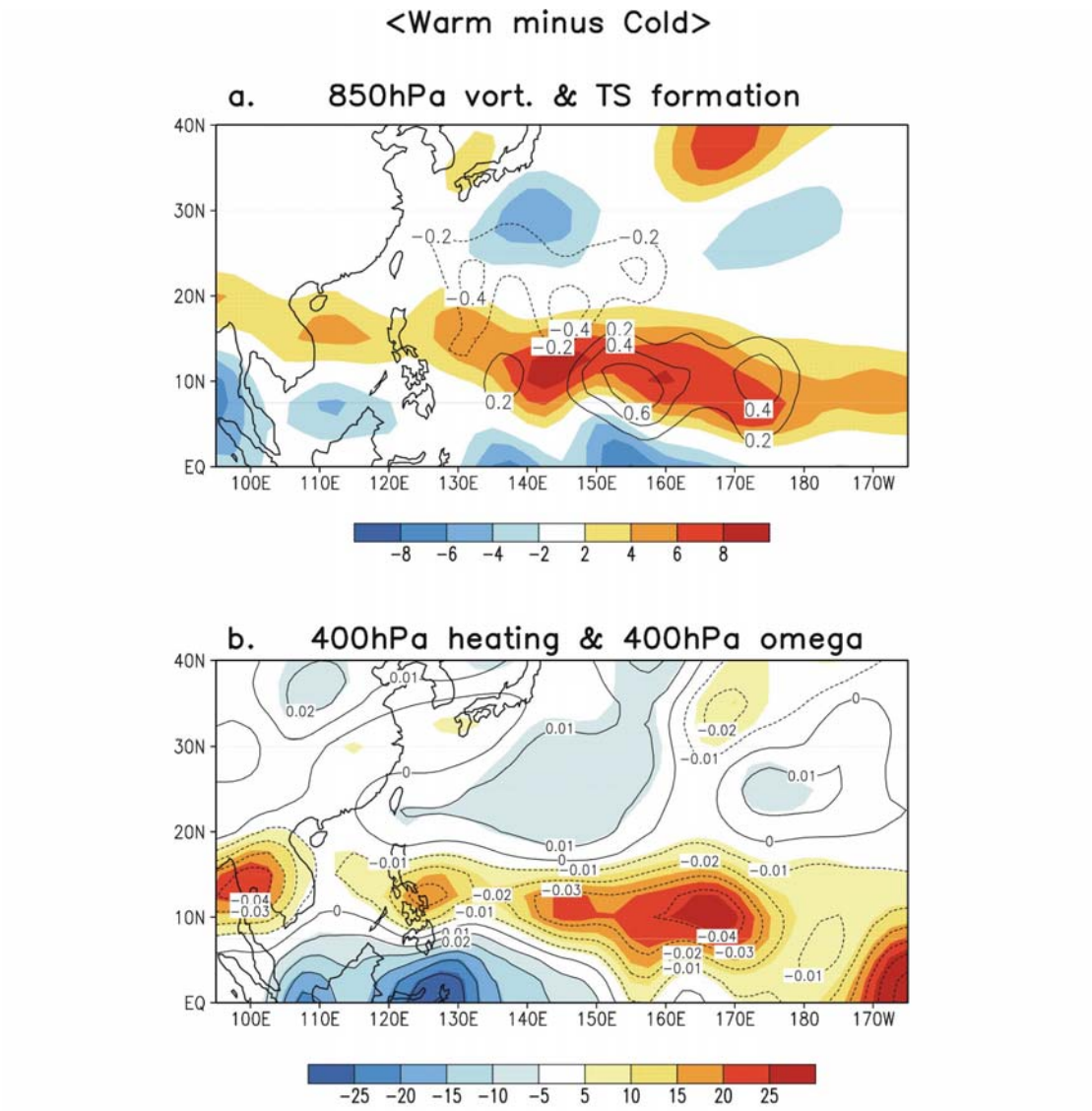

Figure 4.3 (a) 850 hPa vorticity (shaded, unit: 10^{-6} 1/s) and TS formation (contour, unit: numbers per 2.5° longitude/latitude per JAS period) for warm minus cold composites. (b) is same as (b) but for the 400 hPa diabatic heating (shaded, unit 10^{-5}K/s) and 400 hPa pressure velocity (contour, unit: 10^{-2}Pa/s).

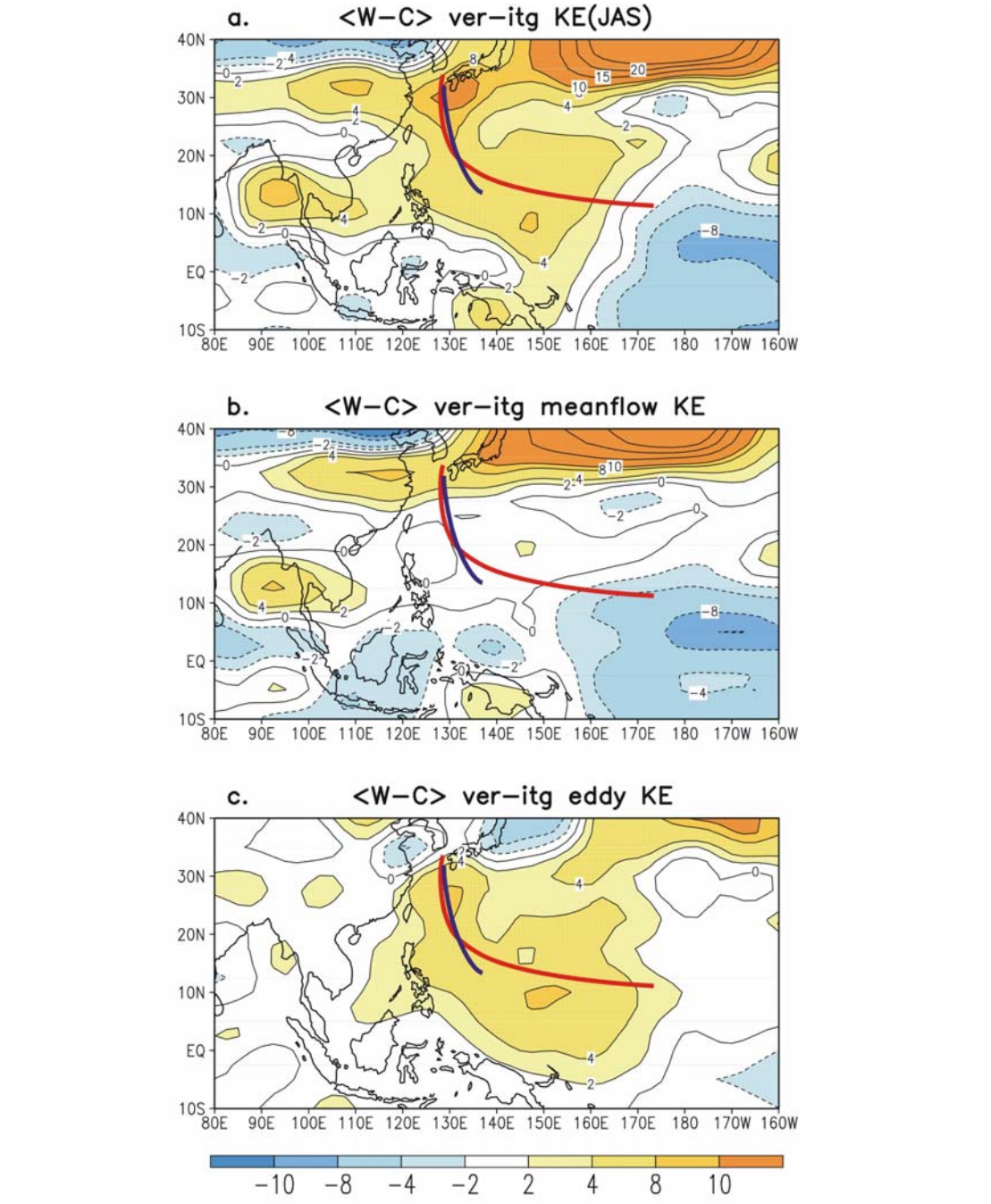

Figure 5.1 Vertically integrated (a) total kinetic energy, (b) mean kinetic energy and (c) eddy kinetic energy for warm minus cold composites. Unit: Jm^{-2}. The red and blue lines are the TS primary tracks of warm and cold composites, respectively.

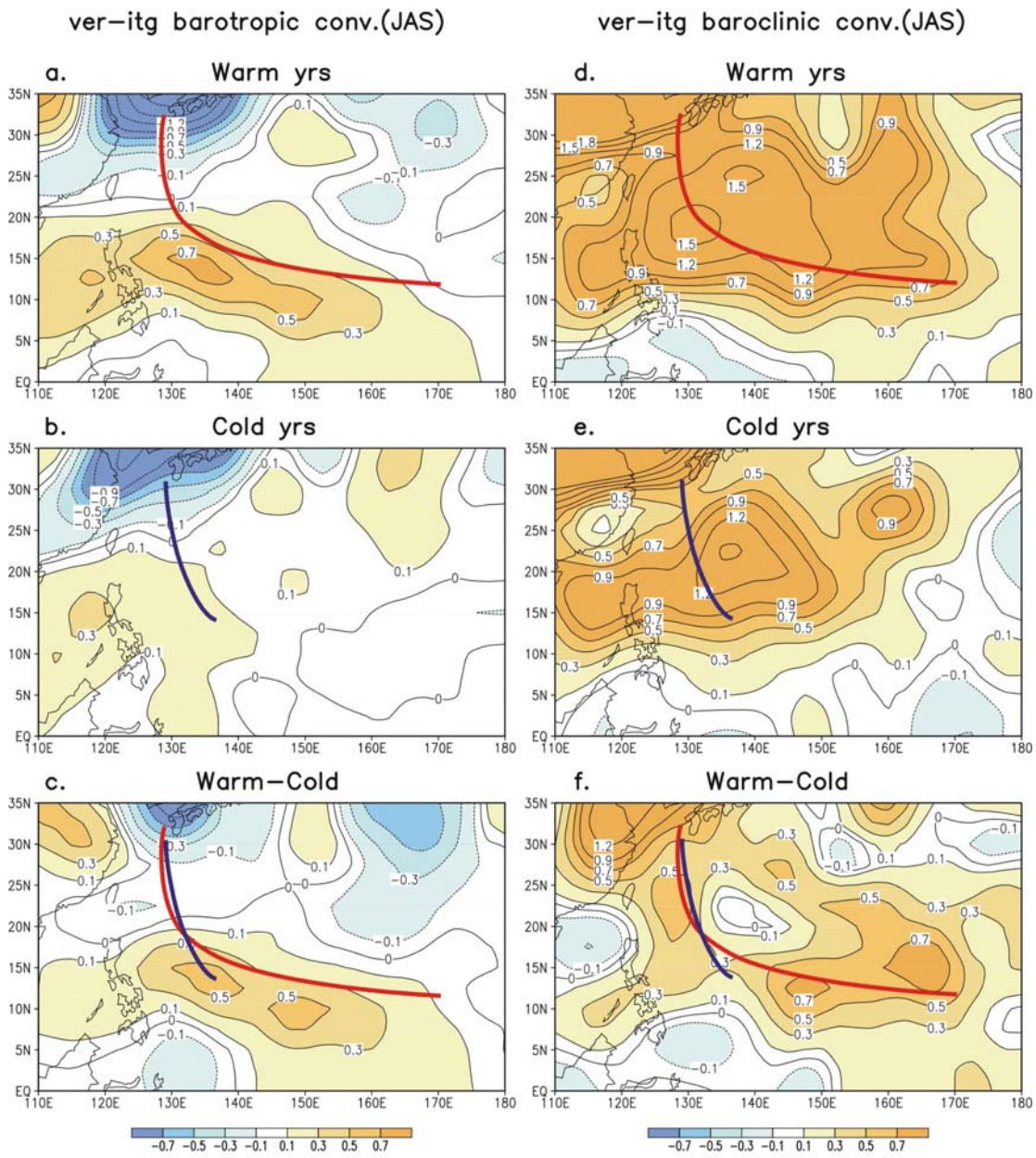

Figure 5.2 Vertically integrated distribution of eddy barotropic energy conversion (Wm^{-2}) for (a) warm composites, (b) cold composites and (c) warm minus cold composites. (d)-(f) are same as (a)-(c), but for the eddy baroclinic energy conversion (Wm^{-2}). The red and blue lines are the TS primary tracks of warm and cold composites, respectively.

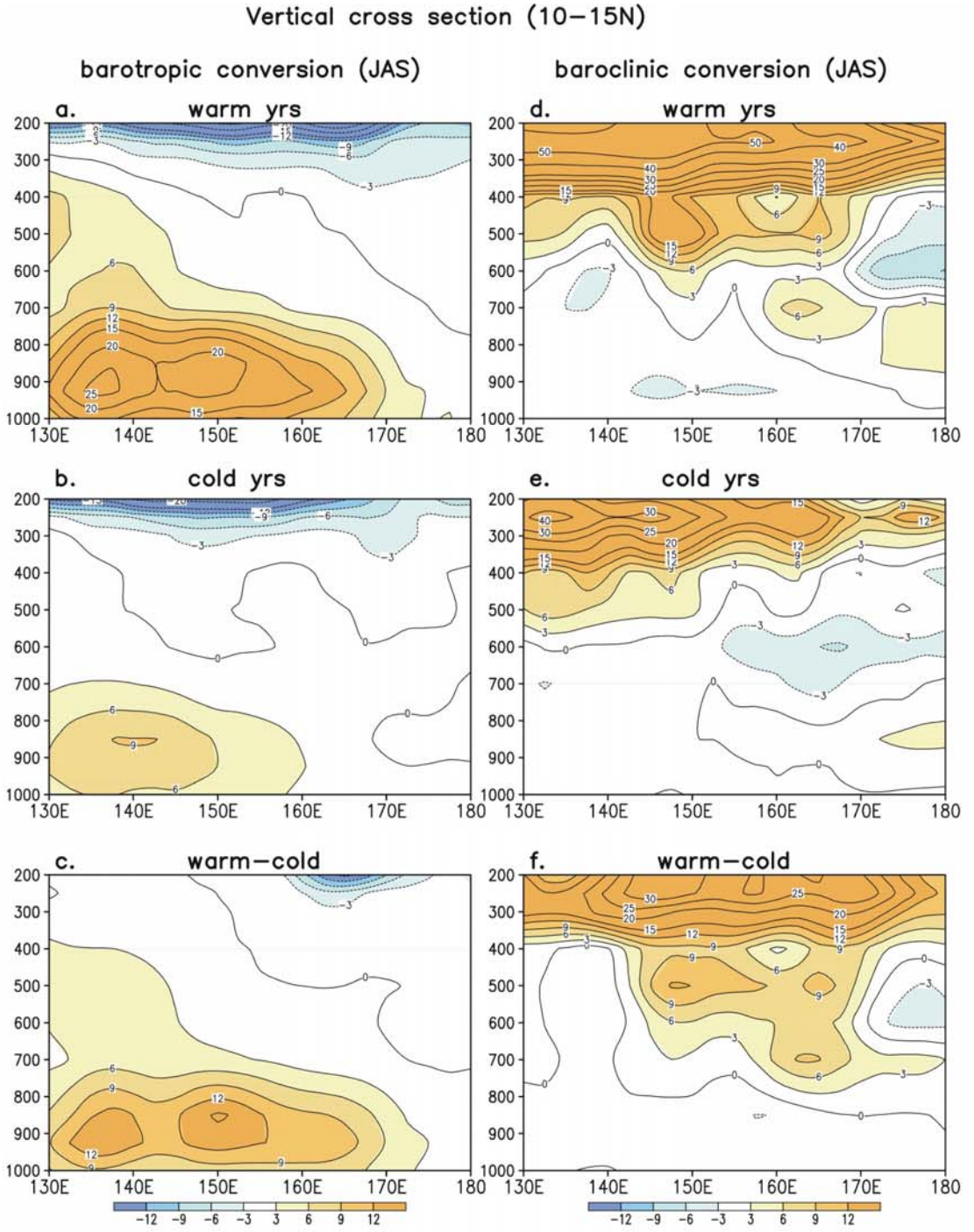

Figure 5.3 Vertical cross sections of eddy barotropic energy conversion for (a) warm composites, (b) cold composites and (c) warm minus cold composites along 10°-15°N. (d)-(f) are same as (a)-(c), but for the eddy baroclinic energy conversion. Unit: $10^{-5}m^2s^{-3}$.

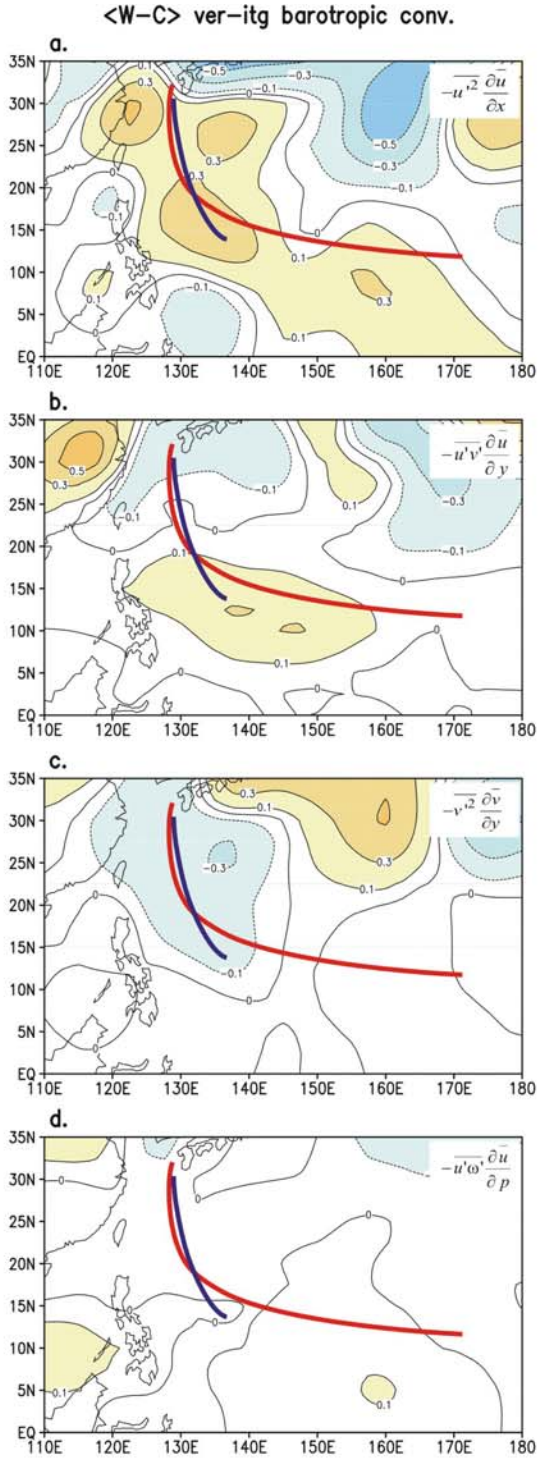

Figure 5.4 Vertically integrated major components ((a) $-\overline{u'^2}\frac{\partial \bar{u}}{\partial x}$, (b) $-\overline{u'v'}\frac{\partial \bar{u}}{\partial y}$, (c) $-\overline{v'^2}\frac{\partial \bar{v}}{\partial y}$ and (d) $-\overline{u'\omega'}\frac{\partial \bar{u}}{\partial p}$) of eddy barotropic energy conversion for warm minus cold composites. Unit: Wm^{-2}. The red and blue lines are the TS primary tracks of warm and cold composites, respectively.

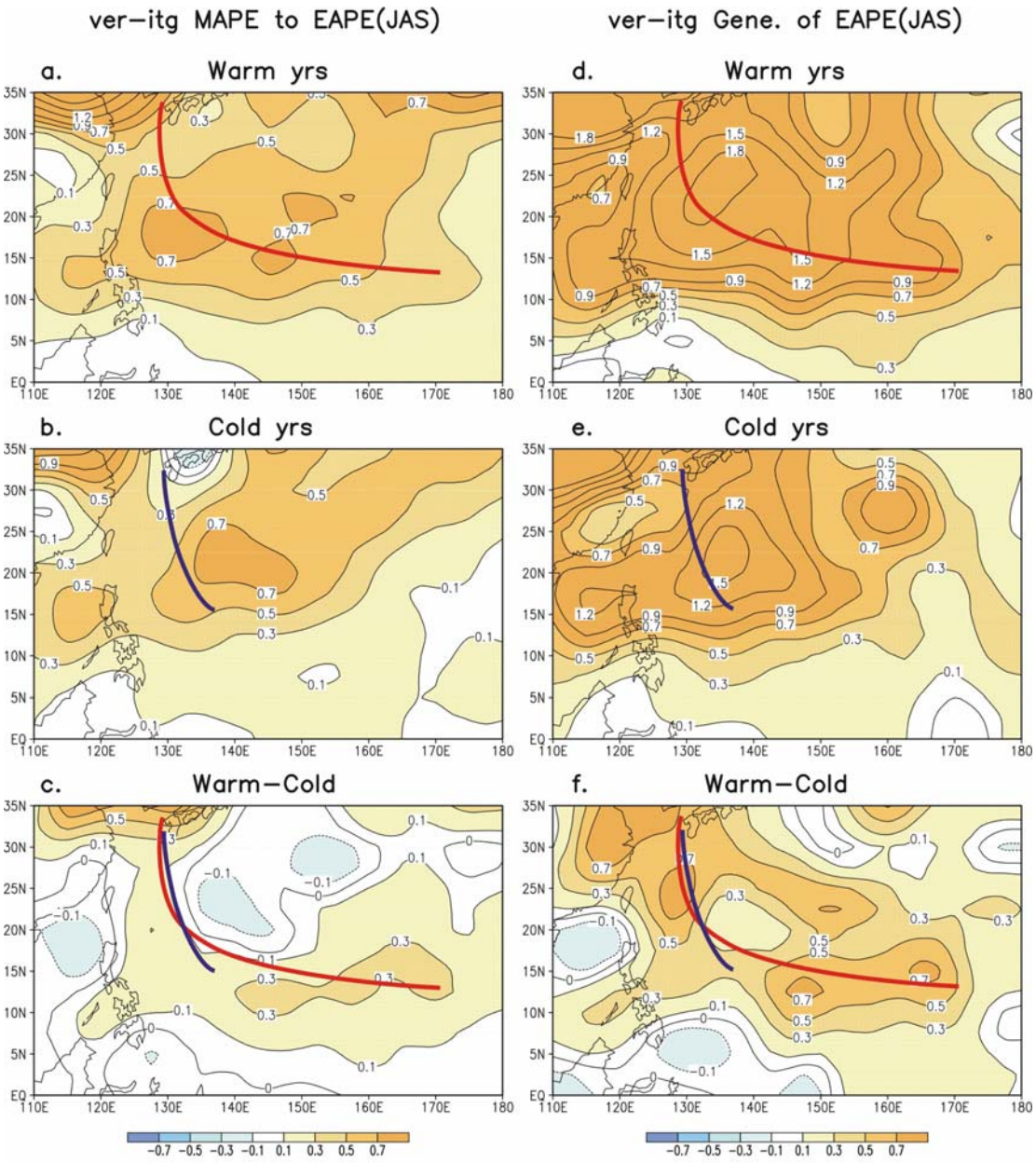

Figure 5.5 Same as Figure 5.2, but for the (a)-(c) MAPE to EAPE conversion, (d)-(f) generation of EAPE. Unit: Wm^{-2}.

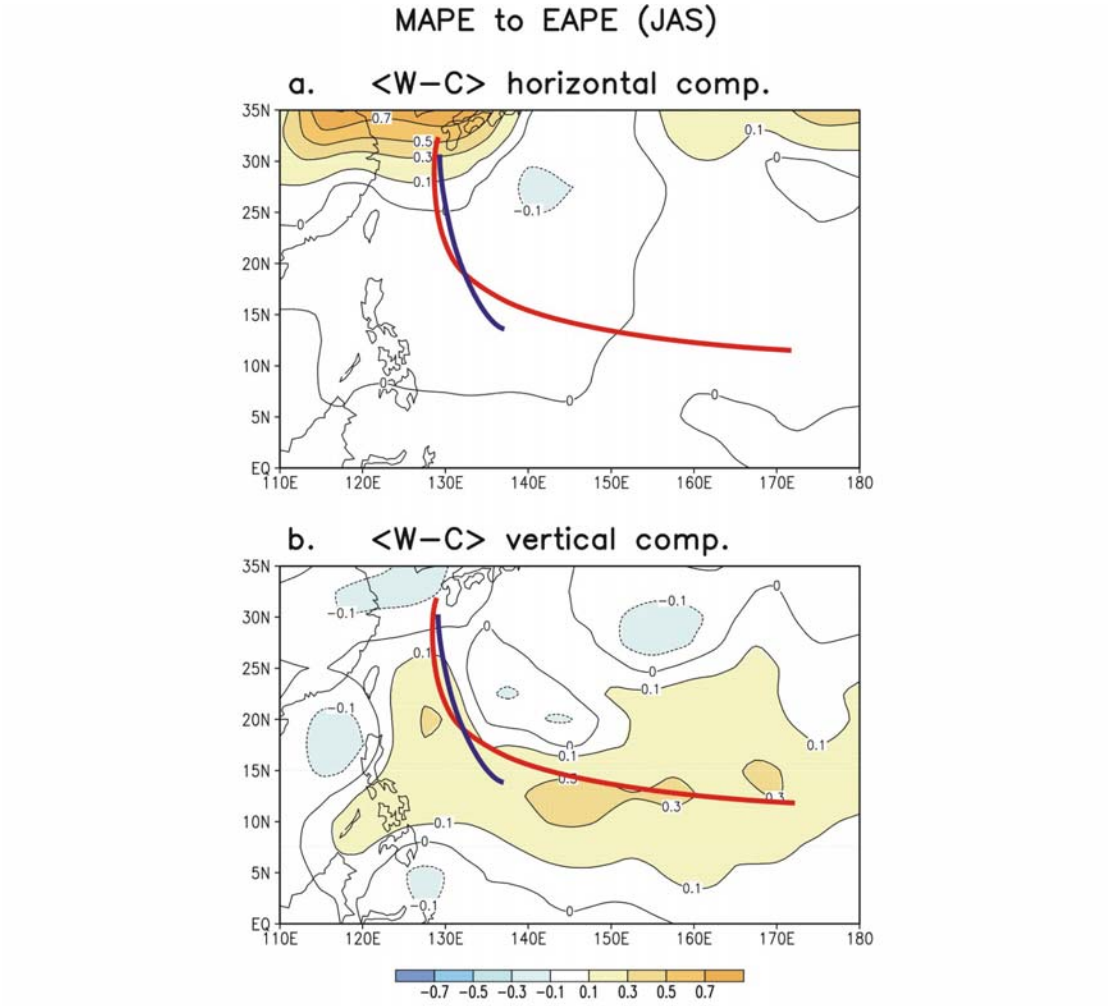

Figure 5.6 Vertically integrated (a) horizontal and (b) vertical component of the MAPE to EAPE conversion for warm minus cold composites. Unit: Wm^{-2}. The red and blue lines are the TS primary tracks of warm and cold composites, respectively.

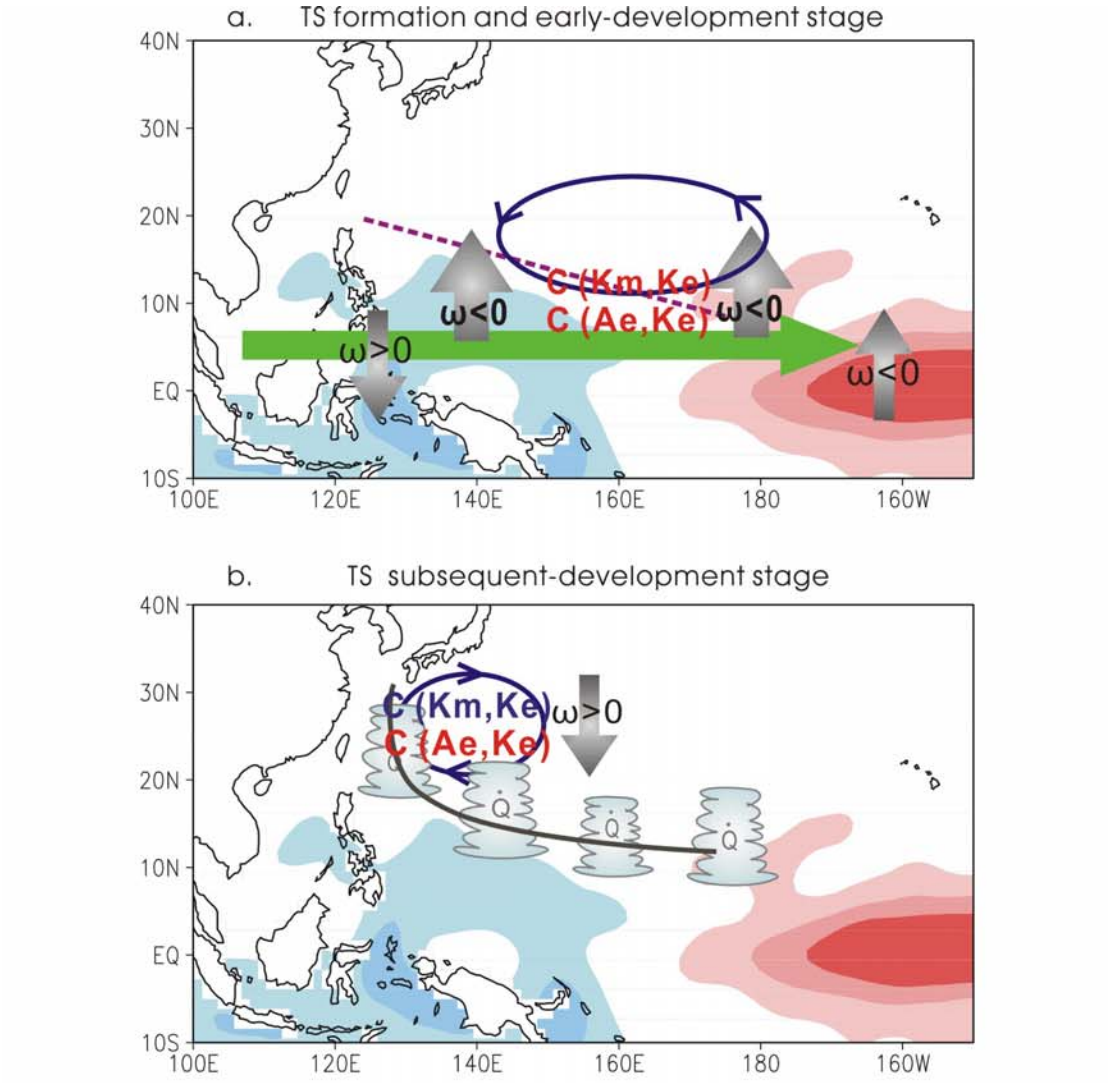

Figure 6.1 Schematic diagram showing the interaction between large-scale circulation and eddy disturbance during (a) TS formation and early-development stage and (b) Subsequent TS development stage for warm minus cold composites. The red and blue shaded regions show the anomalous warm and cold SST, respectively. Cyclonic and anticyclonic circulations represent the anomalous cyclonic and anticyclonic anomalies, respectively. The gray arrows indicate the anomalous vertical motion. The blue cloud with the character Q indicates the anomalous convective disturbance accompanied by diabatic heating. The dashed line in (a) indicates the monsoon trough axis during warm years. The black line in (b) shows the TS track during warm years. Character symbol "C (X, Y)" in red (blue) represents the anomalous positive (negative) energy conversion from X to Y, while Km, Ke, Ae indicate MKE, EKE and EAPE, respectively.

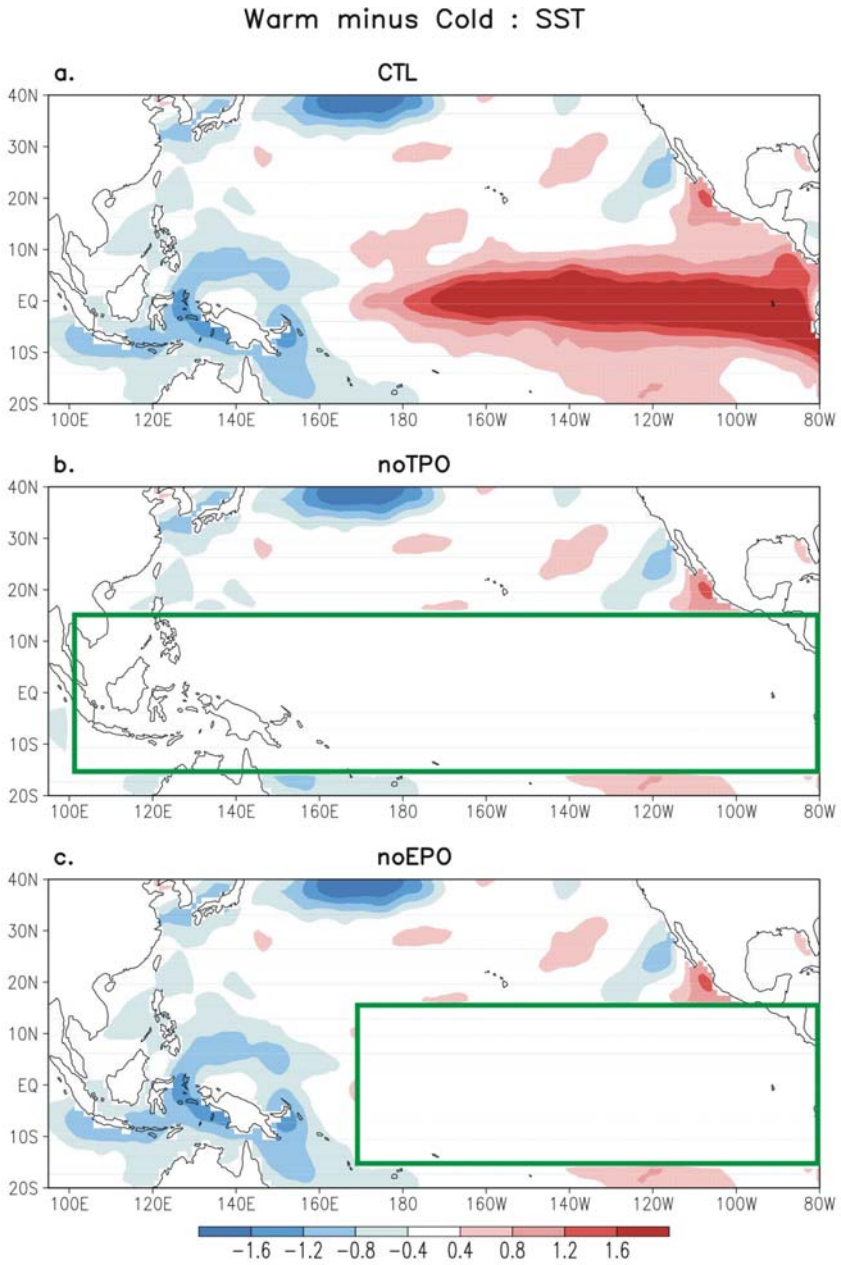

Figure 8.1 Lower boundary conditions for warm minus cold composites in the numerical simulations: (a) CTL, (b) noTPO and (c) noEPO. The climatological SST is used within the box; outside the box, the observed monthly SST is used. Unit: ^{o}C.

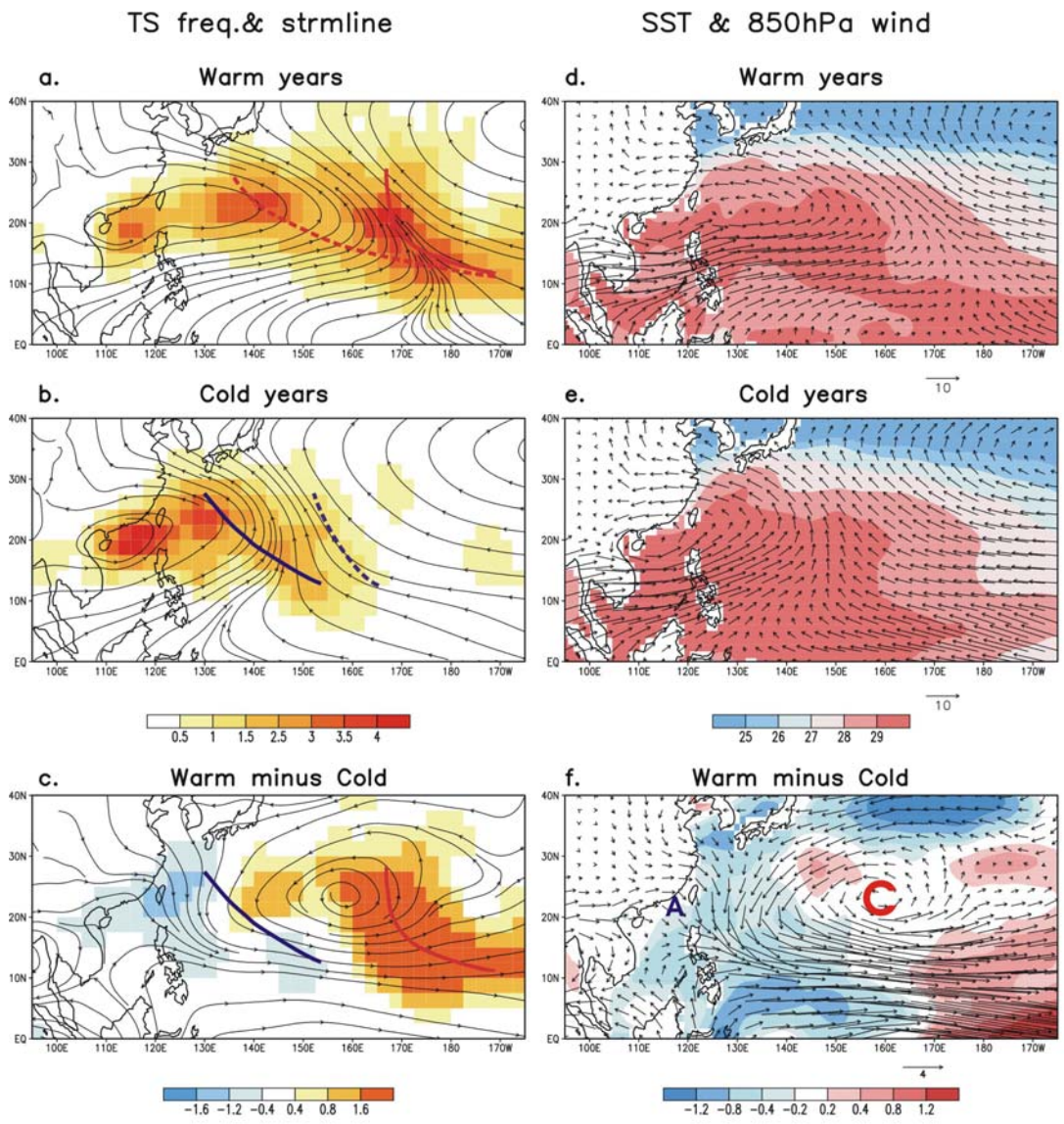

Figure 9.1 Same as Figure 4.1, but for the ECHAM4 CTL experiment.

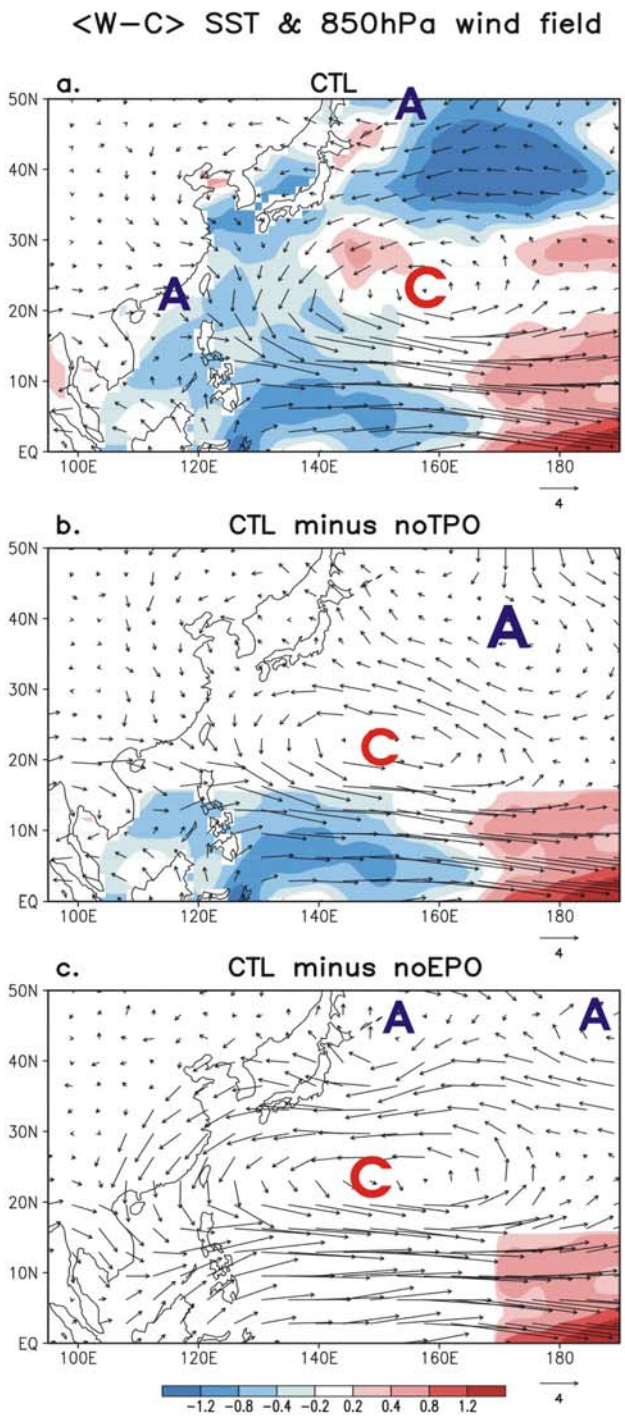

Figure 9.2 SST (shaded, °C) and 850hPa wind fields (vector, m/s) for warm minus cold composites for (a) CTL, (b) CTL minus noTPO and (c) CTL minus noEPO. The characters 〝C〞 and 〝A〞 indicate the cyclonic and anticyclonic anomaly, respectively.

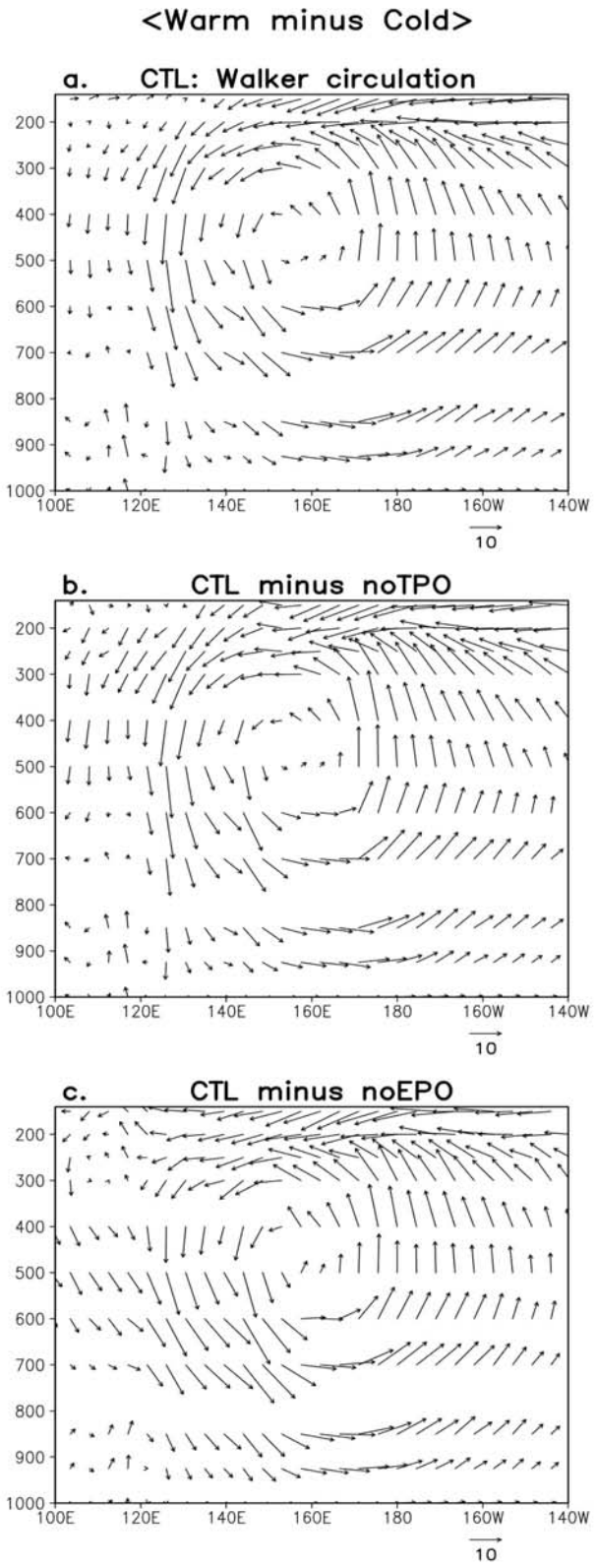

Figure 9.3 Same as Figure 4.2, but for the ECHAM4 numerical experiments: (a) CTL, (b) CTL minus noTPO and (c) CTL minus noEPO.

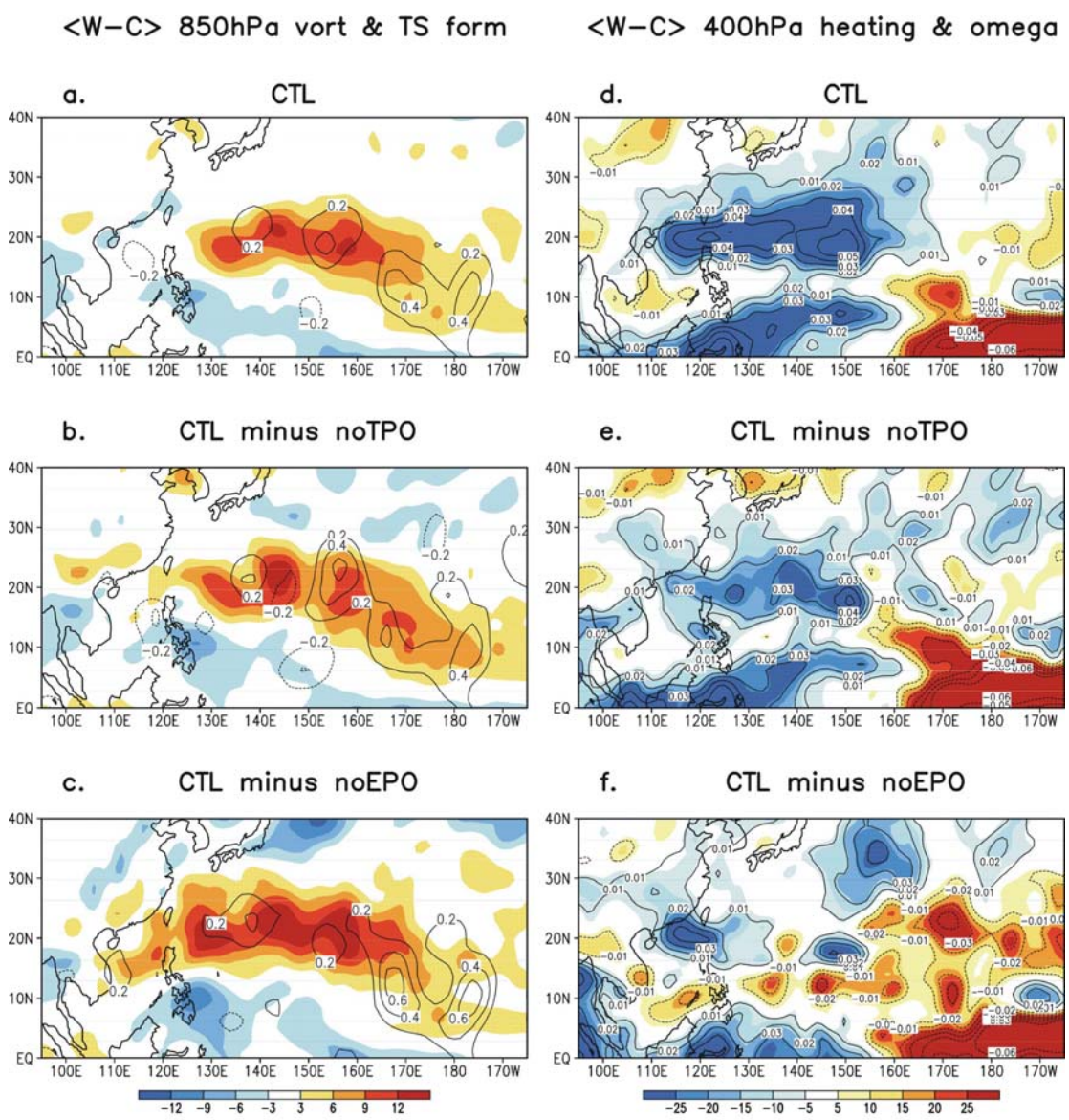

Figure 9.4 Same as Figure 4.3, but for the ECHAM4 numerical experiments: (a) CTL, (b) CTL minus noTPO and (c) CTL minus noEPO.

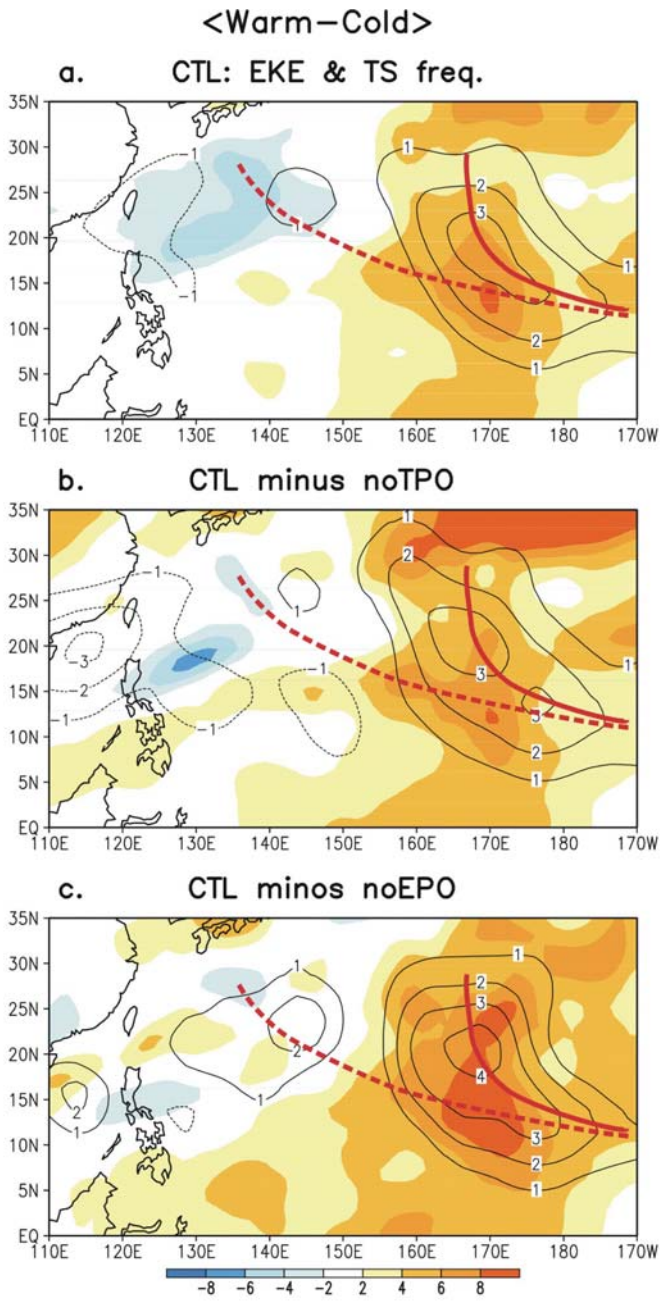

Figure 9.5 Vertically integrated EKE and TS frequency for warm minus cold composites for numerical experiments: (a) CTL and (b) CTL minus noTPO and (c) CTL minus noEPO. The solid (dash) line represents the primary (secondary) track of warm years in the CTL experiment.

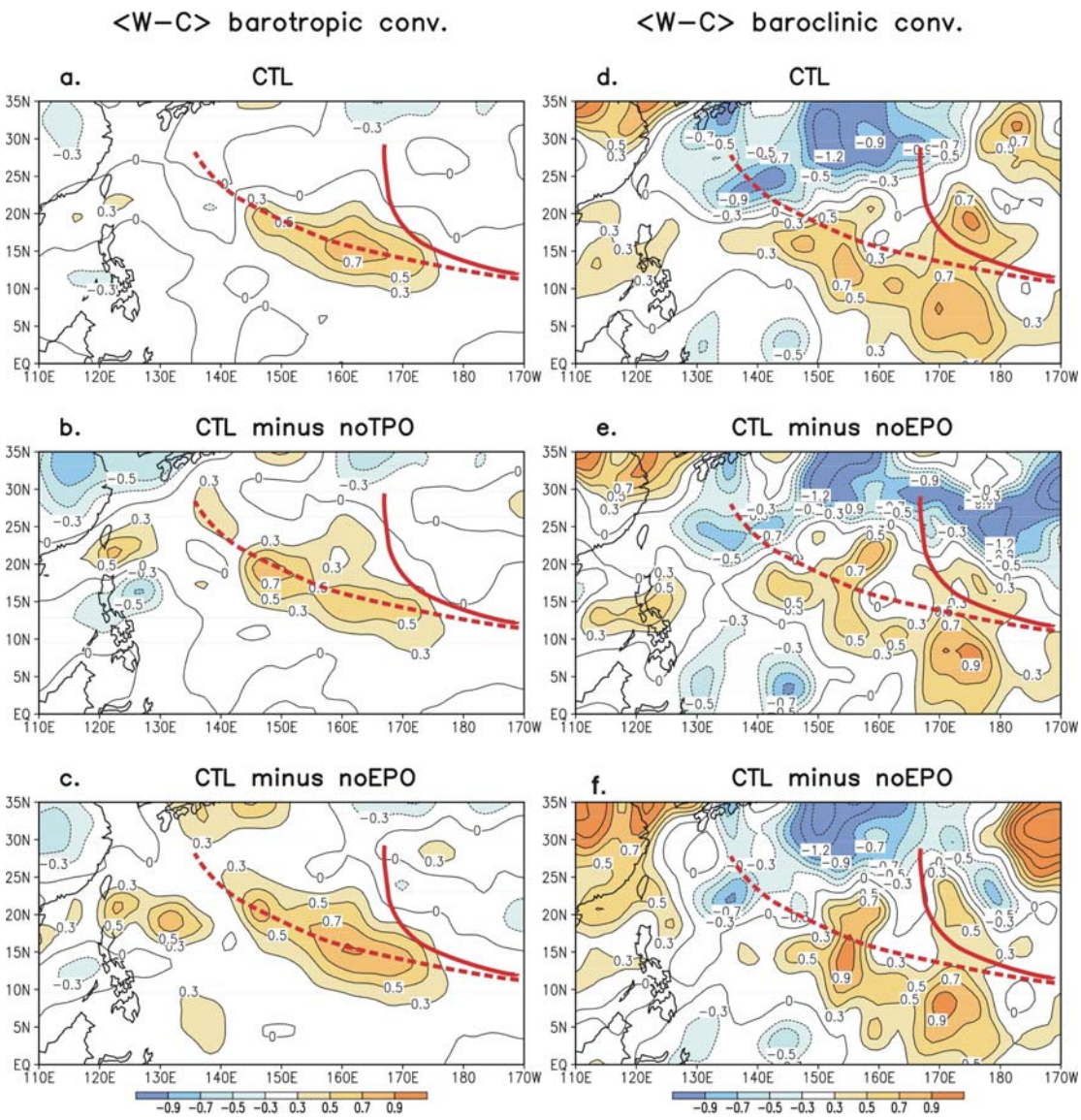

Figure 9.6 Vertically integrated barotropic energy conversion for warm minus cold composites for numerical experiments: (a) CTL and (b) CTL minus noTPO and (c) CTL minus noEPO. (d)-(f) are same as (a)-(c) but for the baroclinic energy conversion. Units: Wm^{-2}. The TS tracks superimposed on each figure are same as Figure 9.5.

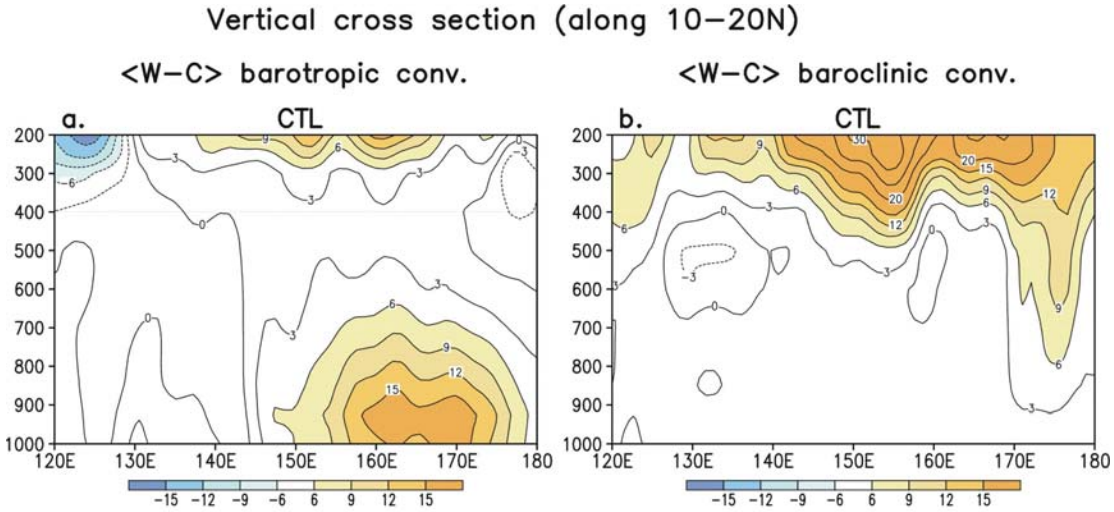

Figure 9.7 Vertical cross sections of (a) barotropic and (b) baroclinic energy conversion along 10^{o}-20^{o}N for warm minus cold composites for the CTL experiments. Unit: $10^{-5}m^{2}s^{-3}$.

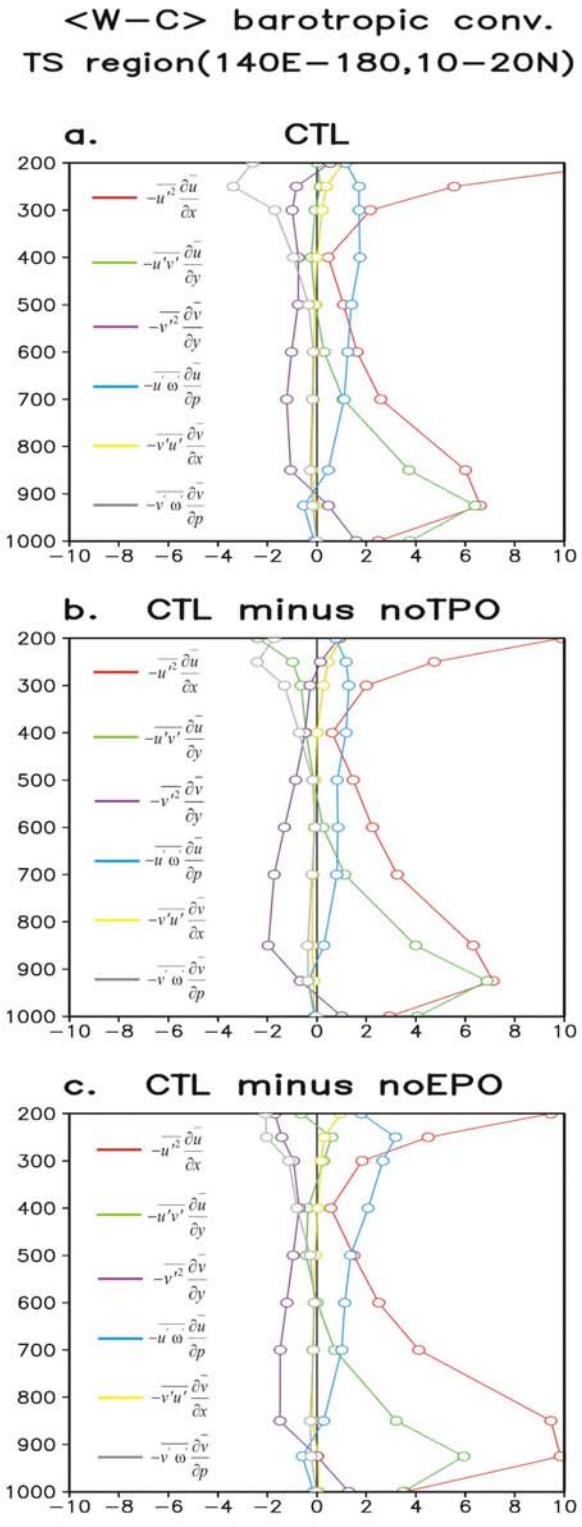

Figure 9.8 Vertical profiles of individual barotropic energy conversion terms for warm minus cold composites over the TS formation and early-development region (140°E-180°, 10°-20°N) for numerical experiments: (a) CTL and (b)CTL minus noTPO and (c) CTL minus noEPO. Unit: $10^{-5}m^2s^{-3}$.

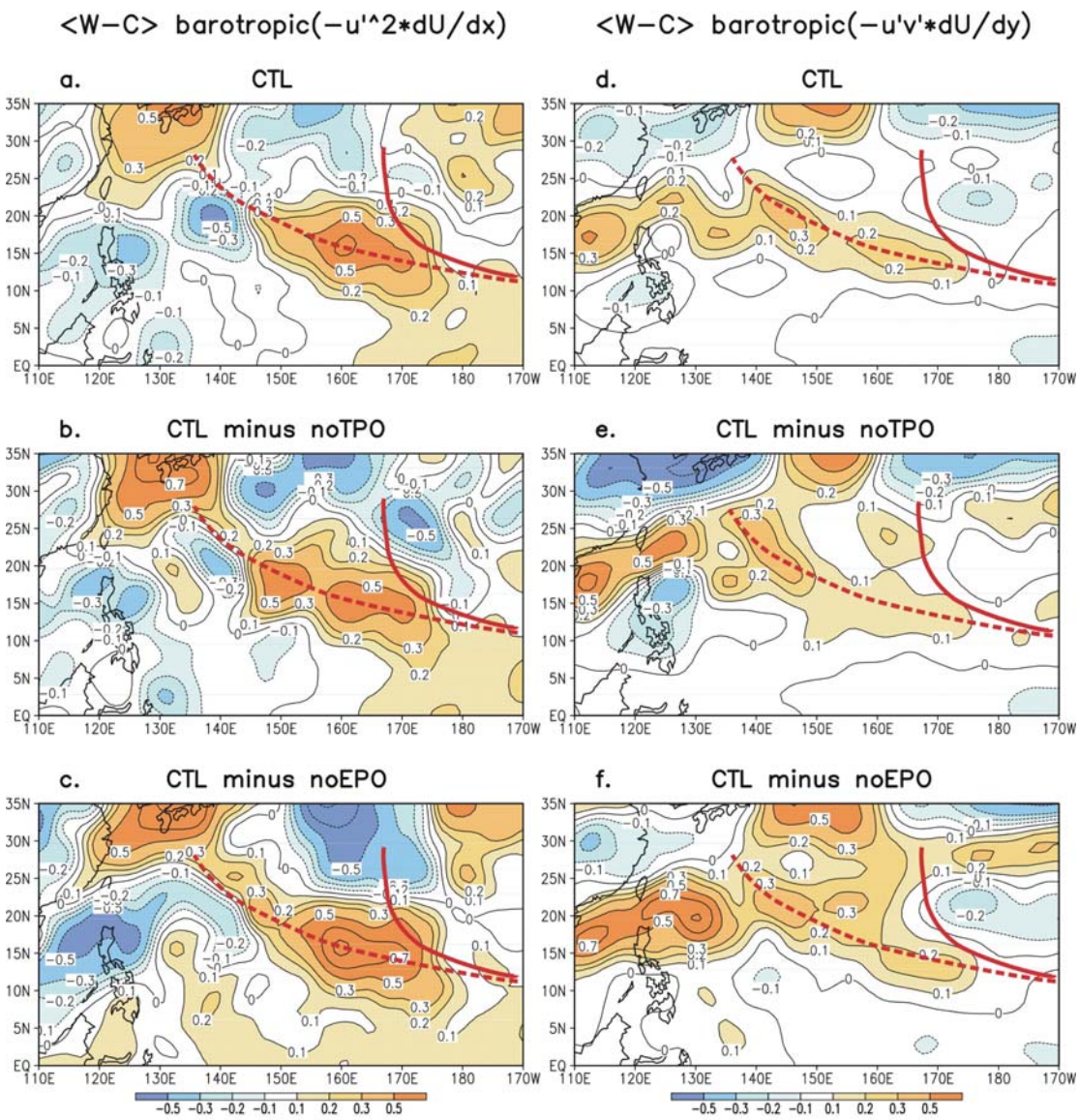

Figure 9.9 Same as Figure 9.6, but for the major components ((a)-(c) $-\overline{u'^2}\frac{\partial \bar{u}}{\partial x}$, (d)-(f) $-\overline{u'v'}\frac{\partial \bar{u}}{\partial y}$) of barotropic energy conversion terms. Unit: Wm^{-2}.

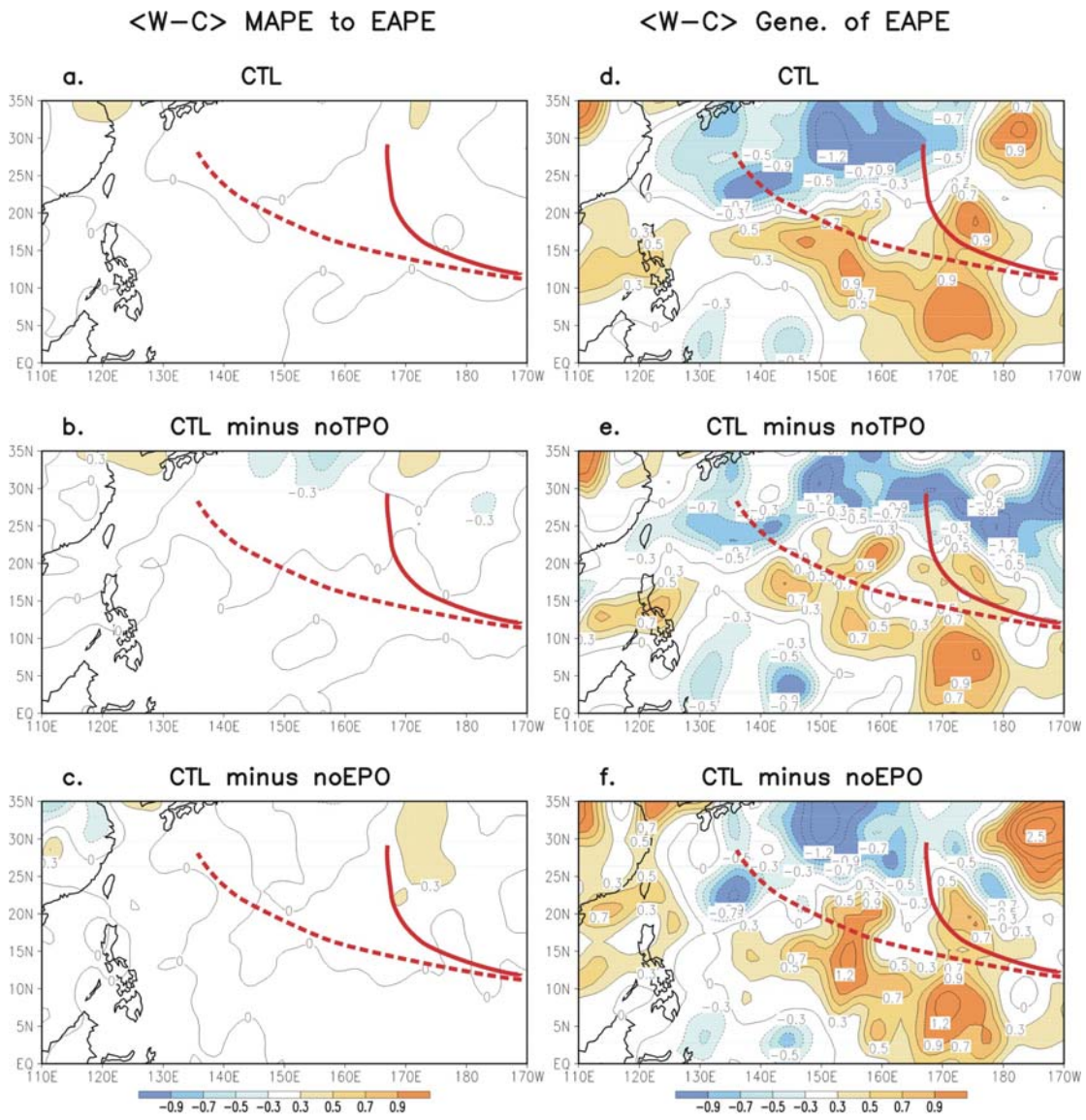

Figure 9.10 Same as Figure 9.6, but for the (a)-(c) MAPE tot EAPE conversion, (d)-(f) generation of EAPE. Unit: Wm^{-2}.

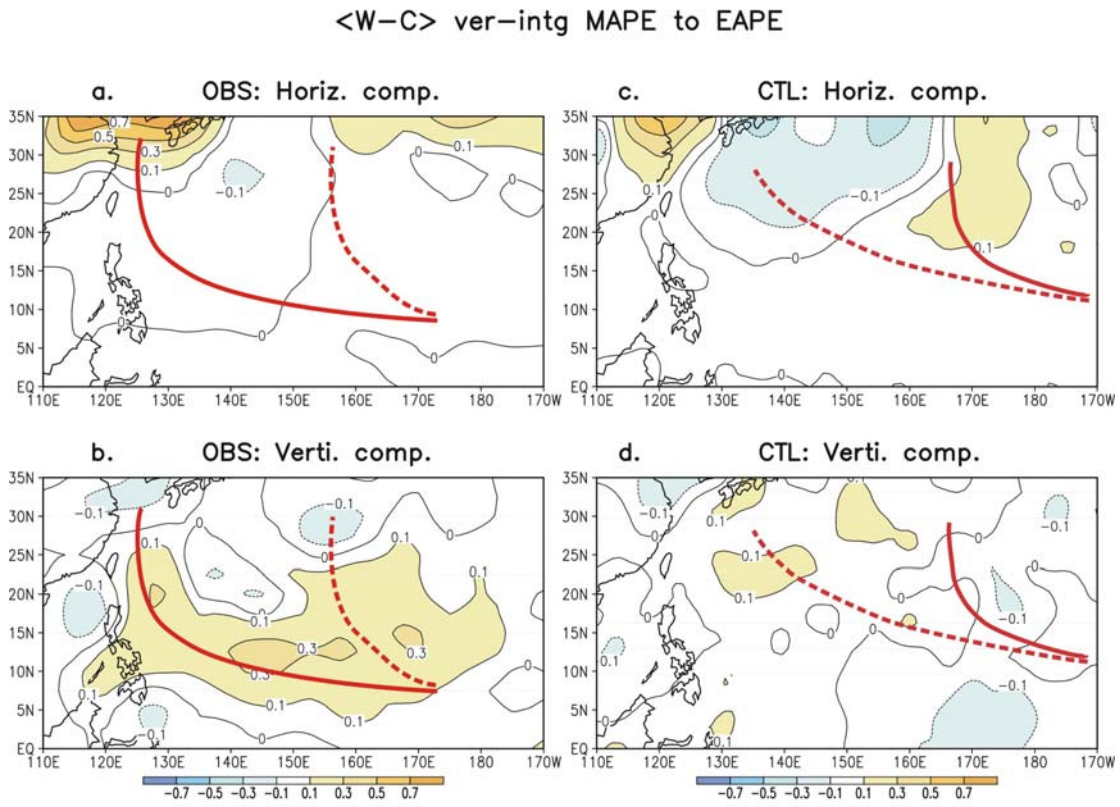

Figure 9.11 Vertically integrated (a) horizontal and (b) vertical components of MAPE to EAPE conversion for warm minus cold composites derived from observation. (c) and (d) are same as (a) and (b), but for the CTL experiment. Unit: Wm^{-2}.